Available online at www.sciencedirect.com
ScienceDirect
Palaeogeography, Palaeoclimatology, Palaeoecology 254 (2007) 561–582
PALAEO
www.elsevier.com/locate/palaeo

Development of the East Asian monsoon: Mineralogical and sedimentologic records in the northern South China Sea since 20 Ma

Shiming Wan [a,*], Anchun Li [a], Peter D. Clift [b], Jan-Berend W. Stuut [c]

[a] Key Laboratory of Marine Geology and Environment, Institute of Oceanology, Chinese Academy of Sciences, Qingdao 266071, China
[b] School of Geosciences, University of Aberdeen, Meston Building, Kings College, Aberdeen, AB24 3UE, United Kingdom
[c] MARUM-Center for Marine Environmental Sciences, Bremen University, Bremen 28334, Germany

Received 22 June 2006; received in revised form 17 July 2007; accepted 18 July 2007

Abstract

We here reconstruct the past change of the East Asian monsoon since 20 Ma using samples from Ocean Drilling Program (ODP) Site 1146 in the northern South China Sea based on a multi-proxy approach including a monomineralic quartz isolation procedure, identification of clay minerals by X-ray Diffraction (XRD) and grain-size analysis of isolated terrigenous materials. Terrigenous supply to ODP Site 1146 was dominated by changes in the strength of multiple sources and transport processes. Grain-size data modeled by an end-member modeling algorithm indicate that eolian dust from the arid Asian inland and fluvial input have contributed on average 20% and 80% of total terrigenous material to ODP Site 1146, respectively. Specifically, about 40–53% of the total (quartz + feldspar) and only 6–11% of the total clay is related to eolian supply at the study site. Detailed analysis of the sedimentary environment, and clay minerals combined with previous studies shows that smectite originates mainly from Luzon, kaolinite from the Pearl River and illite and chlorite from the Pearl River, Taiwan and/or the Yangtze River. The proportion and mass accumulation rate (MAR) of the coarsest end-member EM1 (interpreted as eolian dust), ratios of (illite + chlorite)/smectite, (quartz + feldspar)% and mean grain-size of terrigenous materials at ODP Site 1146 were adopted as proxies for East Asian monsoon evolution. The consistent variation of these independent proxies since 20 Ma shows three profound shifts in the intensity of East Asian winter monsoon relative to summer monsoon, as well as aridity of the Asian continent, occurred at ~15 Ma, ~8 Ma and the youngest at about 3 Ma. In comparison, the summer monsoon intensified contemporaneously with the winter monsoon at 3 Ma. The phased uplift of the Himalaya–Tibetan plateau may have played a significant role in strengthening the Asian monsoon at ~15 Ma, 8 Ma and 3 Ma.

Keywords: East Asian monsoon; South China Sea; Clay minerals; Quartz; Grain size; ODP Leg 184

1. Introduction

The Asian monsoon is the dominant component of the Asian climatic system and its evolution plays a significant role in our understanding of global climate (Webster et al., 1998). Uplift of the Tibetan Plateau has been inferred to be the main cause of monsoon intensification (e.g., Ruddiman and Kutzbach, 1989; Raymo

* Corresponding author. Tel.: +86 532 8289 8535; fax: +86 532 8289 8526.
E-mail addresses: wanshiming@ms.qdio.ac.cn (S. Wan), acli@ms.qdio.ac.cn (A. Li), p.clift@abdn.ac.uk (P.D. Clift), jbstuut@marum.de (J.-B.W. Stuut).

0031-0182/$ - see front matter © 2007 Elsevier B.V. All rights reserved.
doi:10.1016/j.palaeo.2007.07.009

and Ruddiman, 1992; An et al., 2001; Zheng et al., 2004). One way of testing these climate-tectonic models is to define the history and timing of major tectonic and climatic changes in East Asia, including the development of the Asian monsoon. Past fluctuations of the East Asian winter and summer monsoons over long time scales (>1 m.y.) have been studied using the loess–paleosol sequences in the Chinese loess plateau (e.g., An et al., 2001; Ding et al., 2001; Qiang et al., 2001; Guo et al., 2002). By comparison, similar studies of deep-sea sediments in the South China Sea, which is a major sediment sink for fluvial material from the East Asian continent and an ideal location for recording the erosional response to both winter and summer monsoons were hampered by the lack of long sediment cores until six sites were drilled in two areas in the South China Sea during ODP Leg 184 (Wang et al., 2000).

Until now, most of the paleoclimatic studies which permit the reconstruction of long-term evolution of the East Asian paleo-monsoon from sediments in the South China Sea are mainly based on studies of radiolarians (Chen et al., 2003), planktonic and benthic foraminifera (Zheng et al., 2004; Hess and Kuhnt, 2005), stable isotopes (Jia et al., 2003; Jian et al., 2003; Tian et al., 2004) and sediment geochemistry (Wehausen and Brumsack, 2002; Wehausen et al., 2003). Evidence of the enhancement of the East Asian monsoon in the Late Miocene (~8 Ma) and mid-Pliocene (~3 Ma; An et al., 2001; Zheng et al., 2004; Wang et al., 2005) using the mineralogy and sedimentology of sediment in the South China Sea was published in low resolution by Clift et al. (2002), and more recently at high resolution by Clift (2006). However, the latter study is based only on spectral analysis of color data from the core and is not ground truthed.

In this study we use reconstructions of terrigenous accumulation rates at ODP Site 1146 as a proxy for continental erosion, weathering, drying, and transport that can be related to the East Asian monsoon climate. As a result, the sediment record at ODP Site 1146 allows us to test the proposed relationship between growth of the Tibetan Plateau, monsoon evolution, global cooling and enhanced continental erosion. The impact of long-term sea-level changes must also be evaluated when interpreting the accumulation rates of these continental margin sediments, although this effect is modest compared to baselevel changes driven by Tibetan surface uplift.

In this paper, we present a series of independent proxies for paleoclimate derived from terrigenous materials recovered from the South China Sea in order to (1) characterize the mineralogy, grain-size distribution, and mass accumulation rate (MAR) in the sediments of the northern South China Sea since 20 Ma, and (2) reconstruct the long-term history of the East Asian monsoon since 20 Ma, and (3) discuss the possible link of monsoon evolution with Tibetan uplift and/or global ice volume change.

2. Materials and methods

2.1. Materials

ODP Site 1146 is located at 19°27.40′N, 116°16.37′E, at a water depth of 2092 m, within a small rift basin on the mid-continental slope of the northern South China Sea (Fig. 1). Three holes were cored to a sub-seafloor depth of 643 meters composite depth (mcd) (Wang et al., 2000). For this study, a total of 275 samples were sampled continuously at 3 m intervals from 0–327.50 mcd to 499.84–642.44 mcd and at 1.5 m intervals from 327.50 to 498.94 mcd. The lithology of the recovered section changes greatly and is dominated by hemipelagic fine-grained terrigenous materials and nannofossil carbonate ooze. The middle Miocene through Pleistocene section is characterized by relatively carbonate-rich, hemipelagic nannofossil clay. In contrast, the Pleistocene sediments are composed of greenish grey nannofossil clay that is relatively enriched with quartz, feldspar and chlorite (Wang et al., 2000). Terrigenous materials primarily comprise quartz, feldspar, and clay minerals, accounting for up to 99% or more of the clastic fraction. Carbonate contents range from 13% to 64% throughout the section (Wang et al., 2000). Other minor lithologies include low concentrations of diatoms and sponge spicules (average ~2%), observed by microscope.

The chronostratigraphic framework for ODP Site 1146 was established on the basis of the magnetostratigraphy and biostratigraphy (Wang et al., 2000) and then interpolated linearly between control points. ODP Site 1146 is characterized by moderate accumulation rates (average ~3.3 cm/ky), but which increase sharply (9.5 cm/ky) during the Pleistocene. The overall sediment sequences span across approximately the last 19.5 Ma with a sample resolution of about 70.9 ky.

2.2. Methods

In order to determine the most effective paleoclimatic and paleoenvironmental proxy indexes, we carried out a series of chemical procedures, in which we chemically isolated the total terrigenous materials and monomineralic quartz from each bulk sample. Subsequently, the MAR was calculated and grain-size measurements were performed on the extracted terrigenous minerals.

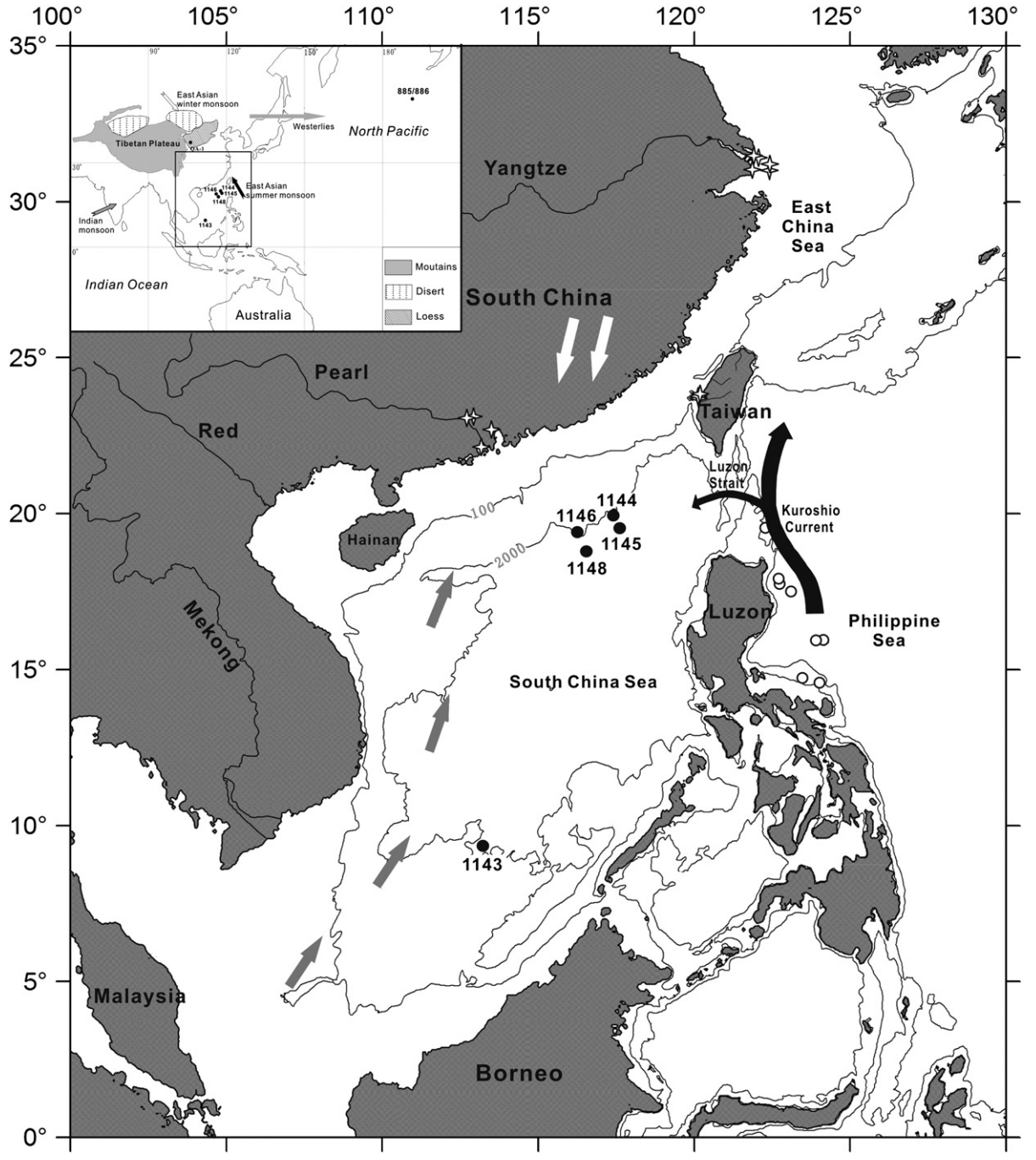

Fig. 1. Locations of geographic features and terrestrial and marine records. The background Map showing ODP Leg 184 drilling sites in the South China Sea, QA-1 loess sequences at Qinan of China, ODP Site 885/886 in the North Pacific mentioned in this paper. The investigated Site 1146 in the northern South China Sea and adjacent landmass are highlighted. −100 m and −2000 m isobaths are shown by grayish line. The location of the river's samples in this study is marked by white stars and 8 core-top samples from the west Philippine Sea by open circles. Gray arrows show modern surface currents during summer monsoon and white arrows during winter monsoon. Black bold arrows indicate the Kuroshio Current.

We modified simple quartz isolation procedures (Kiely and Jackson, 1965; Syers et al., 1968; Dauphin, 1980; Xiao et al., 1995; Sun, 2001), by adding a pre-treatment procedure based on an existing deep-sea eolian extraction procedure (Rea and Janecek, 1981) to our extraction steps. Organic matter, carbonate, biogenic

opal, clay minerals and feldspar were carefully removed using repeatedly excess H_2O_2 (30% at 80 °C), HCl (2.6 mol/L at 80 °C), NaOH (1 mol/L at 80 °C), $KHSO_4$ (heated at 320 °C for 30 min and 650 °C for 45 min) and H_2SiF_6 (30% at 25 °C for 12 h), respectively. These were done in order to calculate the terrigenous grain size and contents in bulk samples, as well as to determine the relative weight percentages of quartz, feldspar and clay minerals within the terrigenous materials. More detailed explanation of our experimental procedures can be found in Wan et al. (2003, 2006).

Minor volumes of sponge spicules, which have suffered crystallization in some samples, were not dissolved in the sample preparation procedure. Fortunately this was not significant for our analysis because the proportion of crystalline spicules in the total sediment is very low (<0.5%) and its interference with the abundant quartz is negligible. Replicate analyses show the uncertainty in quartz content is ±2.37%. Grain-size measurements and scanning electron microscope observations suggest that most of the quartz dissolution in chemical reagents occurs in the <0.8 μm fraction (Wan et al., 2003). In addition, the absolute percentages of quartz, plagioclase and calcite in the bulk samples at ODP Site 1143 and 1144 determined by semi-quantitative XRD methods (Tamburini et al., 2003) are very close to data derived by our methods at ODP Site 1143 (Wan et al., 2006) and 1146 (this study), which further confirms the reliability.

The weight percent of total terrigenous materials, feldspar, quartz, and clay minerals in bulk samples were determined, and the total MAR (g/cm^2/ky) was calculated according to the method of Rea and Janecek (1981) as follows:

$$MAR = LSR*DBD,$$

where LSR = linear sedimentation rates (cm/ky), and DBD = dry bulk density (g/cm^3).

On the basis of the data of LSR and DBD, provided by Wang et al. (2000), the total MAR values were calculated, and in turn the MAR of terrigenous materials, quartz, feldspar, and clay minerals was determined by multiplying the total MAR by the weight percent value of the individual components. Using these accumulation rates, dilution effects by other components were excluded, and furthermore, burial-related sediment compaction was corrected for (Rea and Janecek, 1981).

Grain-size distribution measurements of the extracted terrigenous materials were carried out on a Cilas 940L apparatus in the laboratory of the Institute of Oceanology, Chinese Academy of Sciences (IOCAS),

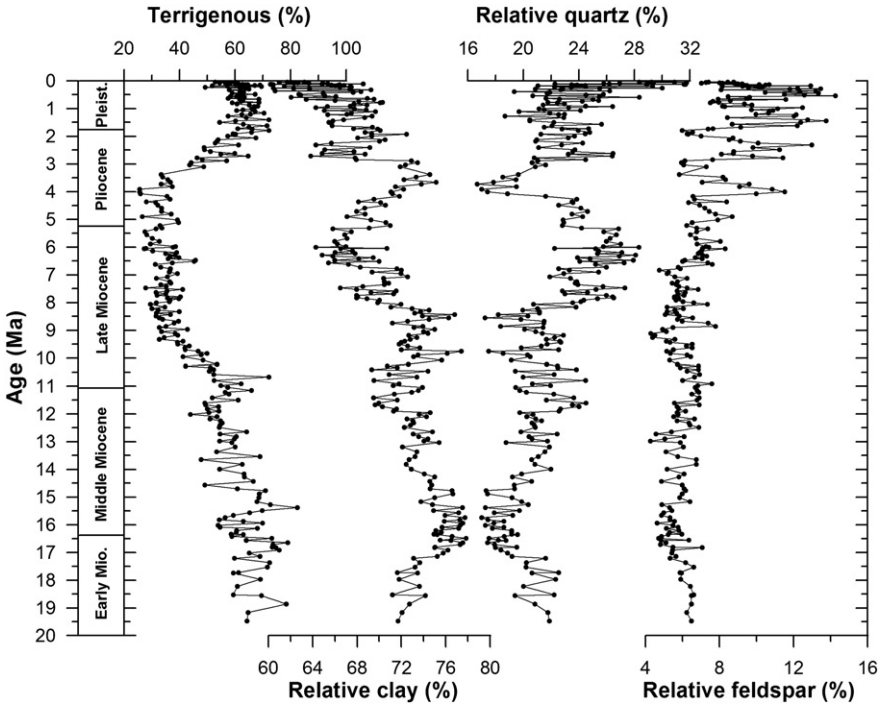

Fig. 2. Variations of weight percents of the total terrigenous materials in bulk samples and relative percents of quartz, feldspar, and clay minerals in terrigenous components at ODP Site 1146 in the northern South China Sea Since about 20 Ma.

Qingdao. Cilas Particle Size Analyzers account for grains in the 0.3 to 2000 μm range. The analytical precision is generally better than 2%. In this study, we applied an inversion algorithm for end-member modelling of compositional data (Weltje, 1997) to the grain-size distributions of the terrigenous materials at ODP Site 1146. This method, developed for the unmixing of multiple-sourced basin fills, is a powerful tool for the unmixing of grain-size distributions that are composed of sediment subpopulations, i.e. end members (e.g., Prins and Weltje, 1999; Prins et al., 2000). The model produces several end members, the number of which depends on the degree of variance. In contrast to other methods for deconvolving mixtures of grain-size distribution, such as factor analysis (e.g., Davis, 1973), end members represent real size distributions, whereas factors or principal components can have negative values without any physical meaning (e.g., Weltje, 1997; Prins and Weltje, 1999).

Because the terrigenous sediment fraction from ODP Site 1146 is very fine-grained (<38 μm), the number of input variables for the end-member model is reduced from 101 to 45 size classes in the range 0.5–38 μm. To estimate the minimum number of end members required for a satisfactory approximation of the data, the coefficients of determination were calculated. The coefficient of determination represents the proportion of the variance of each grain-size class that can be reproduced by the approximated data. This proportion is equal to the squared correlation coefficient (r^2) of the input variables and their approximated values (Weltje, 1997; Prins and Weltje, 1999).

Clay mineral studies were carried out on the <2 μm fraction of the sediment, which was separated based on Stoke's settling velocity principle after removal of carbonate and organic matter by treatment with 10% hydrogen peroxide and 0.5 N HCl, respectively. The analysis was performed on oriented mounts with a D8 ADVANCE diffractometer using CuKα (alpha) radiation (40 kV, 40 mA) in the laboratory of IOCAS. Each sample was measured three times: (1) under dry air conditions (scanning from 3° to 30° 2θ, step size of 0.02°); (2) after ethylene glycol solvation at 100 °C for 1 h (3–30° 2θ, 0.02° steps); and (3) after ethylene glycol solvation at 100 °C for 1 h (24–26° 2θ, 0.01° steps) (e.g., Lamy et al., 1999; Thamban et al., 2002). The last

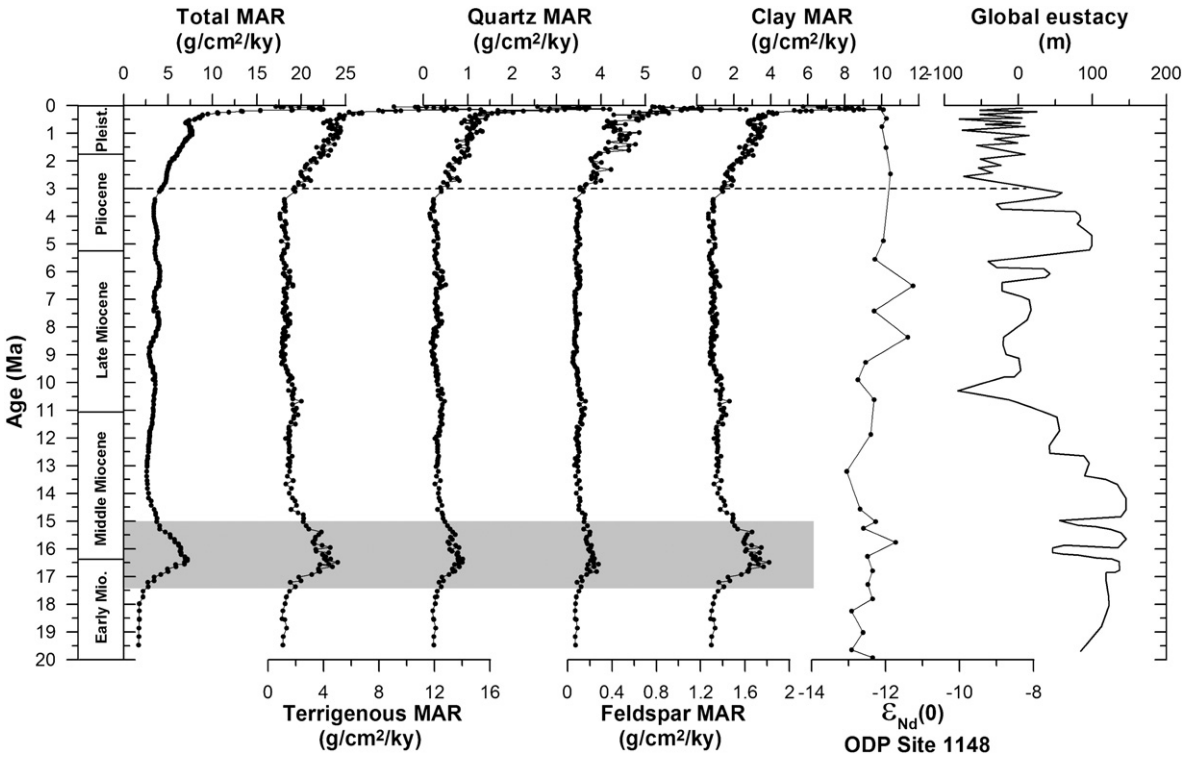

Fig. 3. Variation of MARs of total materials, total terrigenous materials, terrigenous components (quartz, feldspar and clay minerals) at ODP Site 1146 in the northern South China Sea since about 20 Ma. For comparison, the global eustacy curve (Haq et al., 1987) and Nd isotopic variations in sediments at ODP Site 1148 (Li et al., 2003) are also plotted. The sediment pulse between 17.5 and 15 Ma (shaded interval), suggests a violent tectonic activity at that time, which may be related to the cessation of the South China Sea.

was run as a slow scan in order to distinguish the 3.54/3.58 Å kaolinite/chlorite double peak. In addition, some samples were randomly selected to scan following heating at 550 °C for 2 h in order to further identify kaolinite and chlorite, and determinate the existence of smectite and its mixed-layers.

Identification of clay minerals was made mainly using the position of the (001) series of basal reflections on the three XRD diagrams of air drying, ethylene glycol solvation and heating conditions. XRD identified smectite, illite, kaolinite, chlorite and mixed-layer clays. The mixed layer clays are mainly random smectite–illite mixed layers. Smectite–illite mixed layers have small asymmetric peaks between 10 and 14 Å in the air-dried sample, and move to the area between 14 and 17 Å in the glycolated sample, and move to 10 Å in the heated sample. These characteristic peaks of mixed-layer minerals are largely due to random interstratification of smectite with minor illite (R0 order). The mixed-layers proportion in clay minerals for ODP Site 1146 is very low (~2%) and not easy to quantify, which is in good agreement with previous studies in the northern South China Sea (Chen, 1978; Tang and Wang, 1992; Clift et al., 2002). Therefore, we include the small amount of mixed-layer clays in the "smectite" group hereafter. Relative percentages of the four main clay mineral groups were estimated by weighting integrated peak areas of characteristic basal reflections (smectite—17 Å, illite—10 Å, and kaolinite/chlorite—7 Å) in the glycolated state using the Topas 2P software with the empirical factors of Biscaye (1965).

In order to examine the micro-morphology of detrital minerals, especially quartz, we analyzed by a KYKY-2800B scanning electron microscope (SEM) two samples from ODP Site 1146, one sample from the Pearl river mouth, one loess sample from the Loess Plateau and another eolian dust sample collected over the East China Sea. All samples are pretreated with 10% hydrogen peroxide and 0.5 N HCl to remove organic matter and carbonate. In addition, samples from the Pearl river mouth and the Loess Plateau were further treated to isolate the <16 μm fraction of the sediment. This was done in order to analyze a similar grain-size distribution as the terrigenous materials from ODP Site 1146.

3. Results

3.1. Terrigenous components

The weight percent of terrigenous materials in bulk samples ranges from 26% to 72% (Fig. 2). In general, the values of the weight percent of total terrigenous materials in bulk samples are lower between 11 and

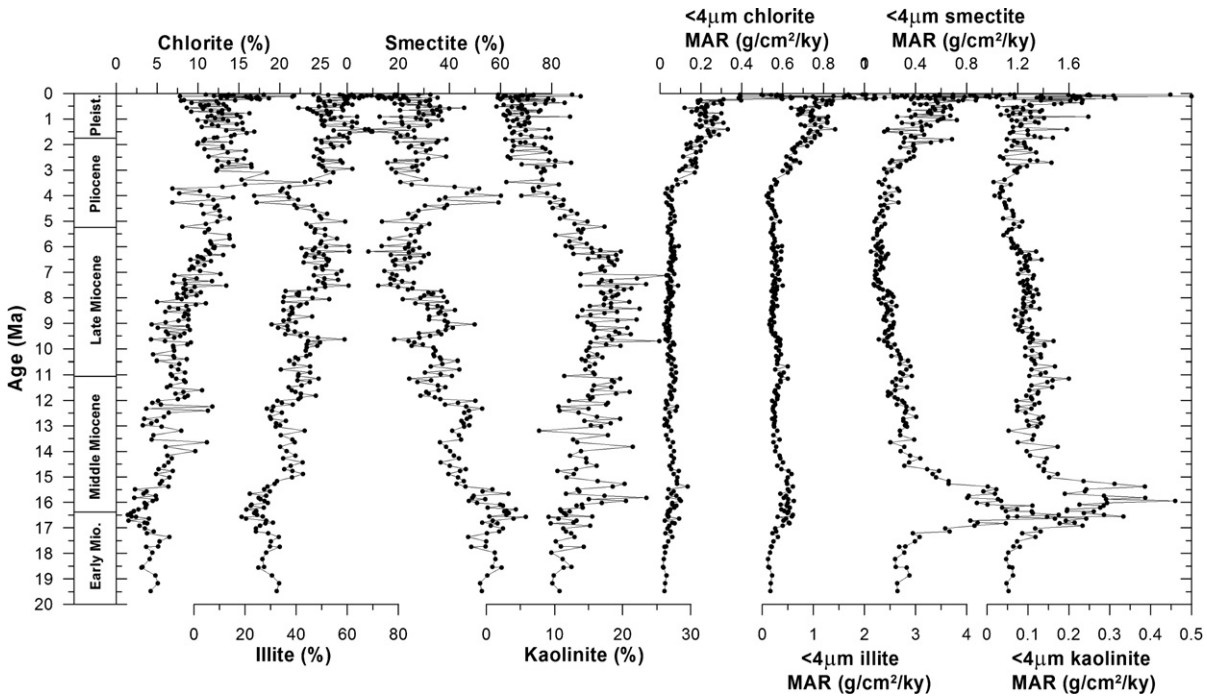

Fig. 4. Variation of clay minerals assemblage and MARs of <4 μm clay minerals at ODP Site 1146 in the northern South China Sea since about 20 Ma. See text for detailed explanations.

3 Ma and higher between 20 and 11 Ma and since 3 Ma. Terrigenous minerals from ODP Site 1146 consist mainly of clay minerals (78–60%), quartz (32–17%) and feldspar (14–4%). As shown in Fig. 2, the relative weight percent of quartz has gradually increased since 20 Ma, the reverse of the clay mineral trend. In contrast, the relative proportion of feldspar shows high-amplitude variation after about 4 Ma.

3.2. Terrigenous mass accumulation rates

Terrigenous MAR at ODP Site 1146 varies in the range 0.9–15.3 g/cm^2/ky, with an average of 3.1 g/cm^2/ky (Fig. 3). In comparison, the MAR of quartz (0.1–4.2 g/cm^2/ky), feldspar (0.05–1.6 g/cm^2/ky) and clay minerals (0.6–10.1 g/cm^2/ky) averages 0.7, 0.3, and 2.1 g/cm^2/ky, respectively. In general, MARs for all terrigenous materials are very low and stable between 20 and 3 Ma, except for a very high MAR interval at 17.5–15 Ma. Strikingly, all terrigenous minerals simultaneously increased since about 3 Ma, reaching a maximum at ~0.15 Ma (Fig. 3).

3.3. Clay minerals

Clay minerals identified consist mainly of illite (19–74%) and smectite (5–70%), with associated kaolinite (2–27%) and chlorite (1–23%). Both chlorite and illite gradually increased since 20 Ma, while smectite decreased. In contrast, kaolinite first became more abundant at 20–7 Ma, but then reduced in importance after 7 Ma (Fig. 4).

3.4. Terrigenous grain size

The average grain-size distribution of all samples shows a bimodal pattern with two modal grain sizes near 2 μm and 9 μm, respectively (Fig. 5A). Fig. 5B shows the coefficients of determination (r^2) plotted against grain size for models with between two and ten end members. The mean coefficient of determination of the grain-size classes increases when the number of end members increases (Fig. 5C). The two-end-member model (r^2_{mean}=0.64) shows low r^2 (<0.6) for the size ranges 4–8 μm and >20 μm. The three-end-member

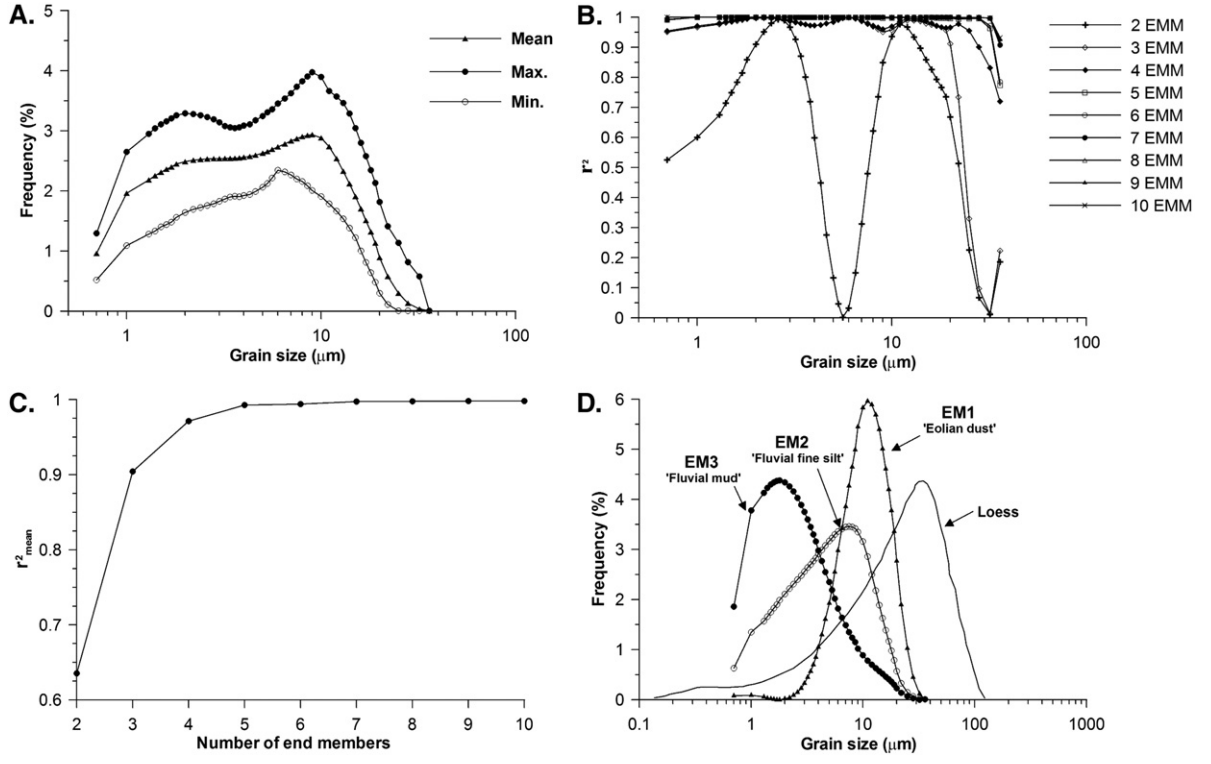

Fig. 5. End-member modeling results of ODP Site 1146. (A) Summary statistics of input data (grain-size distributions, n=273); maximum, mean and minimum frequency recorded in each size class. (B) Coefficients of determination (r^2) for each size class of models with 2–10 end members. (C) Mean coefficient of determination (r^2_{mean}) of all size classes for each end-member model. (D) Modelled three end members of the terrigenous sediment fraction of sediments from ODP Site 1146. For comparison the grain-size distribution of a typical loess sample from Loess Plateau (Sun et al., 2006) is plotted.

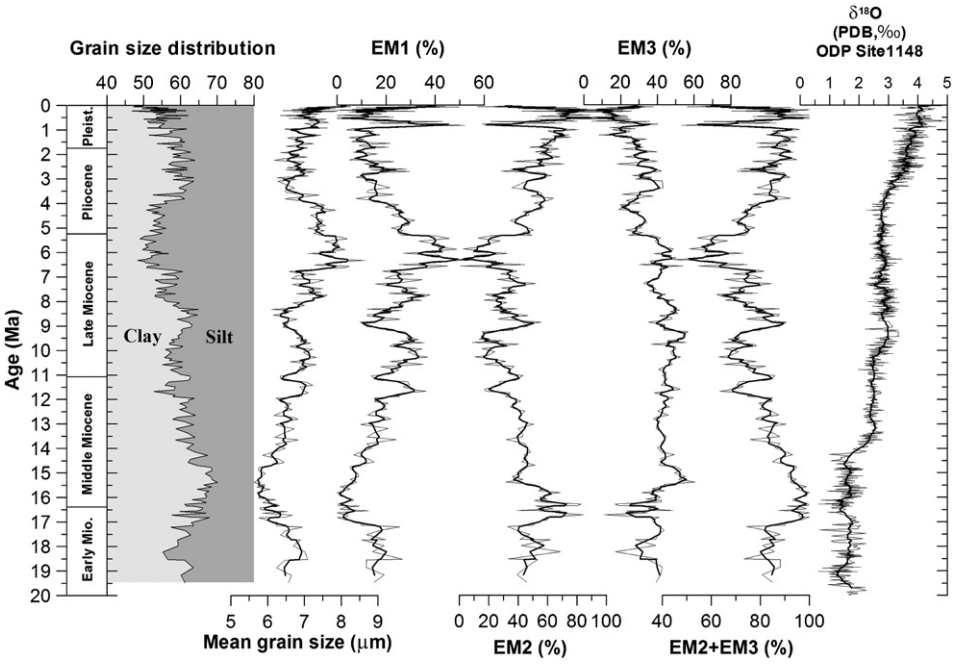

Fig. 6. Variation of grain-size distribution (clay<6 μm, silt>6 μm), mean grain size, and end-member contributions of the terrigenous sediment fraction at ODP Site 1146 since 20 Ma. The benthic $\delta^{18}O$ at ODP Site 1148 (Cheng et al., 2004) is plotted. The data (fine) were smoothed by a three-point moving average (coarse).

model (r^2_{mean}=0.90) shows low r^2 (<0.6) for the size range >22 μm only. The coarse end is only well reproduced by models with four or more end members. In deciding the optimal number of end members, however, the coarse end (>22 μm) can be ignored because it comprises <1.2% weight of the mass. In contrast, the grain-size range 4–8 μm, must be well reproduced by the mixing model because this size range contains a considerable proportion (average 26.8%) of the sediment mass. The goodness-of-fit statistics thus demonstrate that the three-end-member model provides the best compromise between the number of end members and r^2.

Grain-size distributions of the three end members are shown in Fig. 5D. All end members have a clearly defined dominant mode. End-member EM1 has a modal grain size of ~11 μm, end-member EM2 of ~7.5 μm and end-member EM3 has a modal grain size of ~2 μm. The down-core record of grain-size distribution, mean grain size, and the relative contributions of the end members is shown in Fig. 6. End-member EM1 varies between 0 and 56% with an average of 20%, EM2 between 0 and 100% with an average of 44% and EM3 between 0 and 61% with an average of 36%. The variation of EM1 shows a basically similar trend compared to the mean grain size.

4. Discussion

4.1. Sediment sources

Magnetic anomalies indicate that seafloor spreading in the South China Sea dates from the end of the early Oligocene to the early Middle Miocene (~32–16 Ma; Briais et al., 1993). Cenozoic rifting along the South China margin resulted in the proto-South China Sea being consumed under northern Kalimantan and Palawan until the North Palawan block collided with Kalimantan and West Philippines Archipelago at about 17 Ma, thus hindering further seafloor spreading thereafter (e.g., Taylor and Hayes, 1983; Lee and Lawver, 1994; Hall, 2002, Fig. 7). With the cessation of seafloor spreading, the South China Sea basin started to subside as a consequence of thermal relaxation of the oceanic crust (Taylor and Hayes, 1983). The West Philippines Archipelago attached to the North Palawan block and moved further northward and collided with Eurasian margin in the Pliocene (Hall, 2002, Fig. 7).

The main sediment source within the study area is the Pearl River (Fig. 1; Clift et al., 2002; Li et al., 2003). Concomitant with the onset of the seafloor spreading, a large deltaic system of the paleo-Zhujiang (Pearl River) developed and evolved through the Holocene on the

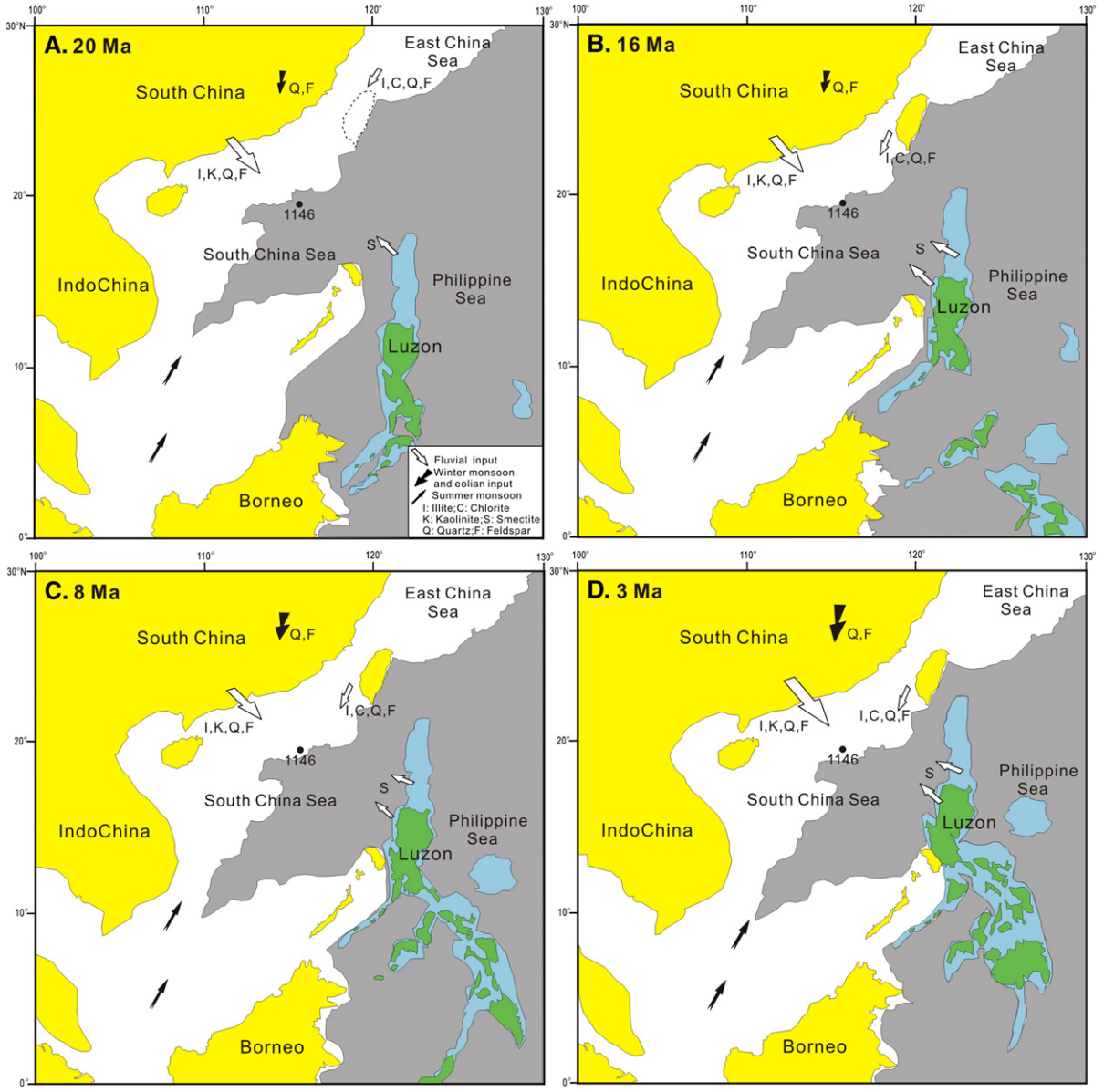

Fig. 7. Schematic diagram showing variation of palaeogeography, relative intensity of fluvial and eolian input to the South China Sea and associated East Asian monsoon intensity at 20 Ma, 16 Ma, 8 Ma and 3 Ma. The distribution of land and sea is modified from Hall (2002). The land is shown by yellow area, shallow sea by white area and deep sea by grey area. Areas filled with green are mainly arc, and cyan submarine arc regions. The 17.5–15 Ma event is characterized by a significant increase of smectite from Luzon islands to the study site in response to the collision of the North Palawan block with the northern Kalimantan and West Philippines Archipelago. A stronger winter monsoon around 8 Ma corresponds to the onset of Asian aridification and increase of eolian dust input and a possible Tibet plateau uplift. A further intensified Asian monsoon at about 3 Ma is expressed by a sharp increase of eolian and fluvial input and illite+chlorite/smectite ratio and quartz–feldspar amounts. See text for detailed explanations. (For interpretation of the references to colour in this figure legend, the reader is referred to the web version of this article.)

northern continental margin of the South China Sea (e.g., Guong et al., 1989). At present, it discharges approximately 69×10^6 tons of sediment annually into its estuary (Milliman and Meade, 1983). The Mekong River is far from the study area and the Red River is mostly shielded from the site by Hainan Island (Fig. 1). The Nd isotopic compositions of sediments from ODP Site 1148 indicate that the source of sediment since 23 Ma is very stable and mainly from South China (Fig. 3) (Clift et al., 2002; Li et al., 2003). The Peal River thus appears to be the main contributor of detrital material to the northern part of the South China Sea.

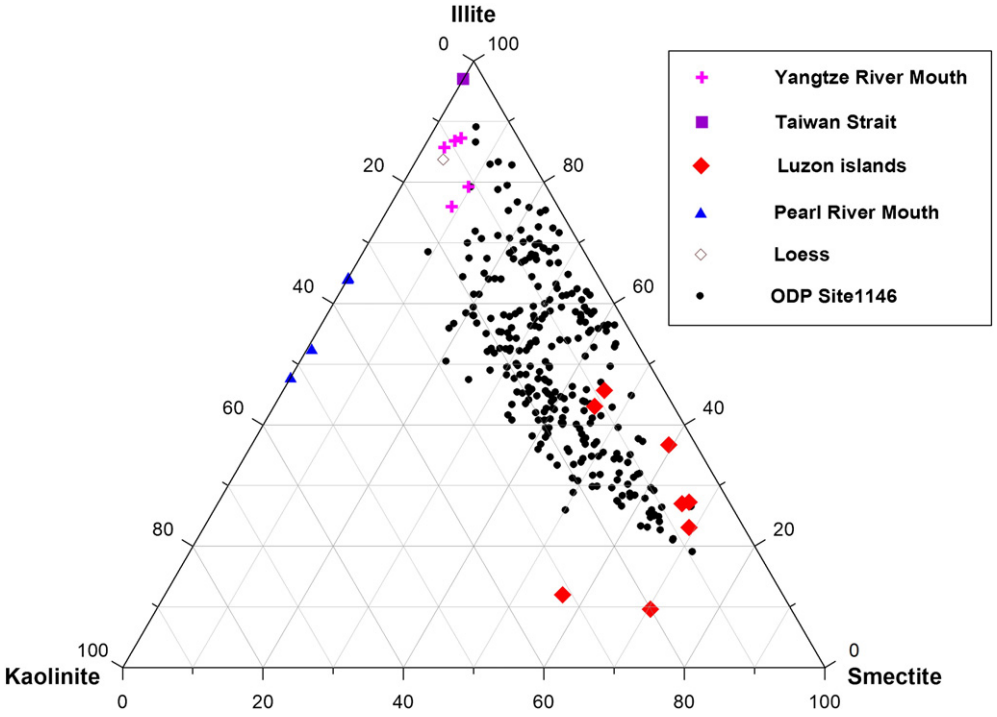

Fig. 8. Ternary diagram showing extent of variation in clay–mineral composition of clays from ODP Site 1146, loess, Yangtze River, Pearl River, Taiwan Strait and Luzon province. Data of loess from Shi et al. (2005).

However, because Nd isotopic values for the Chinese Loess and samples from SW Taiwan lie very close to those of South China and ODP Site 1145 and 1148 (above 480 mcd) (Clift et al., 2002; Li et al., 2003; Boulay et al., 2005), other potential minor contribution such as eolian and Taiwan source cannot be excluded on the basis of the Nd isotope data alone.

The distribution pattern of clay-mineral assemblages in the northern South China Sea is controlled mainly by provenance and reflects the clay mineral composition of two main sources, a northern Asian source (illite–chlorite-rich) and a southern, tropical archipelagic source (smectite rich) (e.g., Chen, 1978). As shown in Fig. 8, clay compositions at ODP Site 1146 are very different from samples from the Pearl River, Yangtze River, Taiwan, and loess, clearly suggesting a mixture of multiple sediment sources. Sediments from ODP Site 1146 contain clay mineral assemblages that are dominated by illite (~45%) and smectite (~34%). In contrast, smectite contents are less than 3% in all river sediments investigated on the Southeast Chinese coast (this study and Boulay et al., 2005) and loess samples (Shi et al., 2005) (Fig. 8 and Table 1). Thus, southern China or the Loess Plateau cannot be the origin of the high smectite clay, which reaches an average of 34% of the clay fraction at ODP Site 1146 (Fig. 4). Smectite is

Table 1
Average clay compositions for sediments from possible sources and ODP site 1146

Province	Number of samples	Chlorite (%)	Illite (%)	Smectite (%)	Kaolinite (%)	Smectite IB	Illite IB
Pearl River	4	8	52	1	39	0.34	0.31
Taiwan	3	30	69	0	1		0.25
Loess	21	20	67	3	10		
Yangtze River	5	16	69	5	9	0.56	0.31
Luzon Island	8	24	21	46	9	1.33	0.33
ODP Site 1146	275	10	45	34	12	1.56	0.37

Note: Clay data of Loess after Shi et al. (2005).

often related to volcanic activity, or to the alteration of volcanic materials by hydrothermal and chemical weathering processes (Chamley, 1989). We analyzed clay mineral compositions of eight core-top samples from the west Philippine Sea and Luzon Strait (Fig. 1). These indicate that smectite percent is between 55 and 35%, with an average of 46%. The abundance of smectite surrounding Luzon is paralleled by the common occurrence of volcaniclastic sediments offshore, suggesting that volcanic rocks are the principle sources for smectite in the surrounding seas (Chen, 1978).

'Crystallinity', a measure of the lattice ordering and crystallite size of clay minerals, is often used to trace possible source regions in marine sediments (e.g., Petschick et al., 1996). The measurements were made by computing the IB (= integral-breadth) of the glycolated 17 Å-smectite and 10 Å-illite peaks. The IB is the width (in $\Delta° 2\theta$) of the rectangle that has the same height and the same area as the measured peak. High values indicate poor crystallinities, low values indicate good crystallinities. IB-values are more sensitive for peak tail variations than the more commonly applied half-height width. IB measurements of smectite are more accurate than the v/p-index (Biscaye, 1965) due to various problems of fixing the background line (Petschick et al., 1996). Our result indicates that the smectite seen at ODP Site 1146 is similar to those from the Luzon area because it has poor crystallinity. It is very different from the Chinese Rivers that show good crystallinity (Table 1). In comparison, there is no clear difference of IB values of illite from different regions. Therefore, we can conclude that the Luzon arc, including large volumes of basalt, is the main contributor of smectite to the northern South China Sea, and thus to the study site.

Based on experimental comparison, the total percentage of particles <4 μm analyzed by the Cilas 940L laser apparatus is approximately equivalent to the 2 μm boundary with pipette analysis. Then 14% smectite in the <4 μm terrigenous materials is calculated, based on the <4 μm clay fraction (~42%) by grain-size analyses, and smectite proportion (~34%) by XRD analysis. It is known that the various clay minerals have different size distributions and that smectite generally has the smallest particle size, extending from 0.9 μm to below 0.1 μm (Gibbs, 1977). This was also confirmed by SEM-EDS for the smectite in sediments of ODP Site 1146 (Wan, 2006). Therefore, we estimate that the Luzon Arc has contributed about 14% of the lithic fraction to the study site since 20 Ma, assuming all the smectite was from Luzon.

Taiwan is an active mountain belt evolved from the middle Miocene (16–15 Ma) through the Quaternary and to the present (Huang et al., 2006) and may have been a considerable source of sediments to the northern South China Sea (Shao et al., 2001; Liu et al., 2003; Boulay et al., 2005). Samples from Taiwan contain high proportions of illite (50–60%) and chlorite (30–40%), and negligible contents of smectite and kaolinite (Chamley et al., 1993). This result is consistent with our XRD data from three samples near the Chuoshui River mouth of Taiwan (Fig. 1 and Table 1). In comparison, the Yangtze River suspended sediments, with a similar clay assemblage as that from Taiwan (Table 1), has also been suggested as a sediment source for ODP Site 1146 (Liu et al., 2003). However, sediment flux from the Yangtze is blocked by the perennial northward-flowing Kuroshio Current and the low water depth in the Taiwan Strait. We conclude that flux from the East China Sea probably has only had a limited participation in the South China Sea since the middle Miocene. In contrast, Taiwan did not exist in the early Miocene and thus suspended materials from the East China Sea could have been transported along the Chinese coast to the northern South China Sea by the winter coastal current at that time (Fig. 7). Therefore, we support the conclusion of Liu et al. (2003) that smectite at ODP Site 1146 likely comes from the Luzon arc, illite and chlorite mainly from the Pearl River and Taiwan/Yangtze and kaolinite from the Pearl River.

In addition, a number of studies have suggested that the South China Sea has received eolian silts and clays (loess) during glacial climate phases (e.g., Wang et al., 1999b). However, it is very difficult to constrain the eolian contribution because of the terrigenous nature of the hemipelagic sediments that blanket the northern continental slope (Wang et al., 2000) and the quantitative identification of eolian dust in the northern South China Sea has previously been missing. Here, we try to identify wind blown and fluvially derived sediment fractions at ODP Site 1146 by unmixing the grain-size distributions of the land-derived sediment fraction using an end-member algorithm (Weltje, 1997). The end-member model indicates that three end members produce the optimal balance between statistical description of the variance in the data set and the complexity of the mixture composition. As shown in Fig. 5D, the three end members consist of unimodal particle-size distributions. In previous studies (e.g., offshore Namibia), the coarsest two end members were usually interpreted as 'coarse eolian dust' and 'fine eolian dust' and the finest end member as 'fluvial mud' (Stuut et al., 2002; Stuut and Lamy, 2004). In this study, the coarsest end-member EM1 and the finest EM3 can also be interpreted as eolian dust and fluvial mud, respectively. However, it is not accurate to ascribe the middle end-member EM2 as

fine eolian dust because EM1 plus EM2 can reach 64% proportion of the terrigenous materials at ODP Site 1146. The major terrigenous sediment source must be fluvial input, with eolian dust only accounting for a small proportion of the total (Wang et al., 1999b, 2000; Li et al., 2003; Clift et al., 2001). A 5% eolian contribution to ODP Site 1145 in the northern South China Sea was roughly estimated based on the modern mineral aerosol flux value (0.5 g/cm^2/ky) (Duce et al., 1991) and the mean terrigenous MAR at the study site (Boulay et al., 2005). Therefore, the middle end-member EM2 can be considered as being of fluvial origin.

In contrast, Boulay et al. (2007) employed the end-member modeling method for grain-size analysis of sediment recovered at ODP Site 1144 and dating back to 1.1 Ma. These authors interpreted variations in the coarse member to reflect the effect of sea-level variations. However, there are different factors controlling terrigenous sedimentation over tectonic and orbital time scales and we believe that the coarse member EM1 modeled from grain-size data of ODP Site 1146 since 20 Ma is not the effect of seal-level change, but instead the signal of eolian dust. This is because the clastic flux to the Asian marginal seas over tectonic time scales is mostly controlled by the erosional response to monsoonal precipitation and topographic uplift of Tibet, not to global eustacy (Rea, 1992; Clift, 2006). Specifically, the absence of any similarity between EM1 MAR and global eustacy (Fig. 9) clearly suggests that the coarse member EM1 does not represent the effect of sea-level change. Furthermore, the grain-size distribution of the typical loess from the Lingtai section of the Chinese Loess Plateau (Sun et al., 2006) is plotted for comparison (Fig. 5D). The eolian character of EM1 is suggested by the agreement between the grain-size distributions of EM1 with the typical loess sample. The grain-size distribution of the loess onshore is coarser probably due to the fact that it has undergone significant sorting from the source to core site. The surface texture, as seen by SEM, of some quartz grains from sediments at ODP Site 1146 shows clearly subangular to subrounded shape and collision pits, which are typical eolian evidence (Sun and An, 2000) and very similar to loess from the Loess Plateau and dust over the East China Sea (Fig. 10). In contrast, quartz grains from the Pearl River mouth are characterized by an irregular, angular appearance and sharp edges. Although we have not tried to quantify the contents of eolian grains by SEM, there is no doubt that many eolian minerals have been deposited at ODP Site 1146. The average terrigenous MAR since 20 Ma is

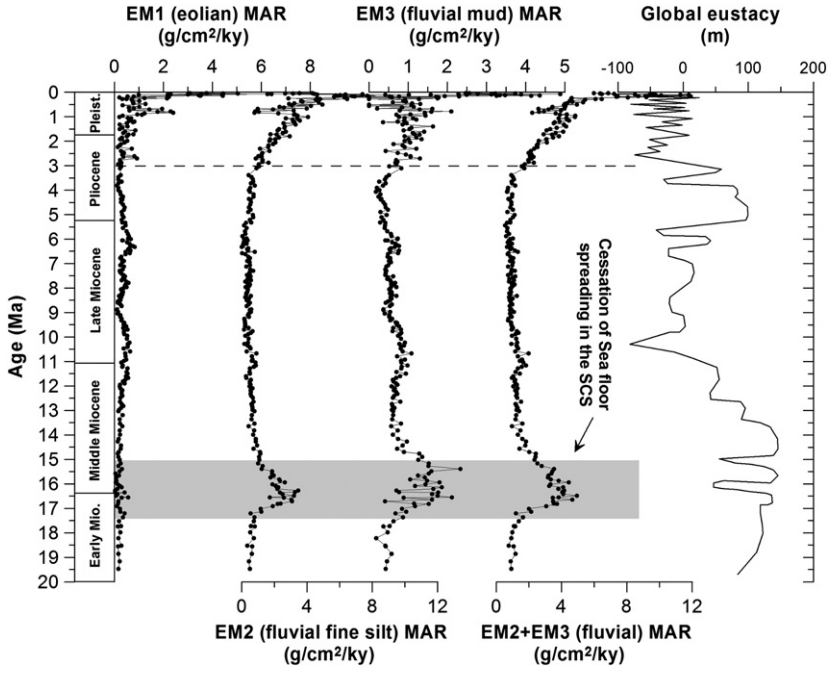

Fig. 9. Variation of mass accumulation rates of three end members at ODP Site 1146 in the northern South China Sea since about 20 Ma. Note that EM1 (eolian) MAR has no pulse between 17.5 and 15 Ma (shaded interval), which is on the contrary to MARs of finer end-members EM2 and EM3 (fluvial origin). The dashed line marks the simultaneous increasing of three end-member MARs since about 3 Ma. For comparison, the global eustacy curve (Haq et al., 1987) is plotted.

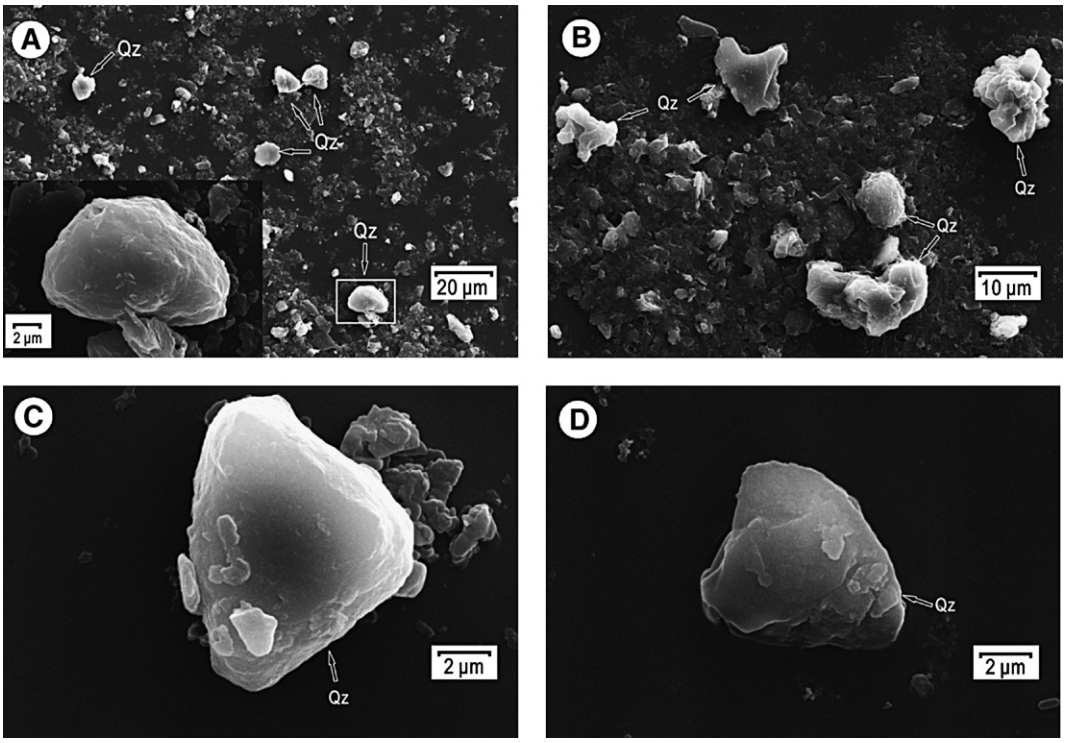

Fig. 10. SEM images of samples from (A) ODP Site 1146, (B) the Pearl river mouth, (C) the Loess Plateau and (D) the eolian dust over the East China Sea. Magnified image from the box in (A) showing the quartz grain with typical eolian evidence.

about 3.2 g/cm^2/ky. Assuming a mineral aerosol flux equal to, or less than, the estimated modern value (0.5 g/cm^2/ky) (Duce et al., 1991), the maximum eolian contribution to the terrigenous flux accounts for ~16%, which is very close to the end-member EM1 proportion (~20%) for the terrigenous materials calculated from the grain size. In addition, there is further evidence to support this interpretation. The collision of the North Palawan block with Kalimantan and the West Philippines Archipelago at about 17 Ma caused seafloor spreading in the South China Sea to cease (e.g., Taylor and Hayes, 1983; Lee and Lawver, 1994). As shown in Fig. 3, the remarkable high MARs of terrigenous minerals between 17.5 and 15 Ma suggests that a dramatic tectonic phase occurred at this time, which may be related to cessation of seafloor spreading. In addition, there is a distinct change in elemental composition in sediments at ODP Site 1148 during that time (Li et al., 2003; Shao et al., 2004). All these observations suggest that the end of seafloor spreading in the South China Sea is a period of strong tectonic activity, which induced intensified continental erosion and increased river load to the northern South China Sea. If the interpretation of the coarsest end-member EM1 as eolian dust is correct, then the MAR of end-member EM1 should not increase between 17.5 and 15 Ma because eolian input would not be influenced by local tectonic activity. Just as our interpretation, EM1 MAR shows no increase between 17.5 and 15 Ma, in contrast to MARs of the finer end-members EM2 and EM3 (fluvial origin) (Fig. 9).

Besides clay minerals, quartz and feldspar are also important components (average ~30%) in the terrigenous sediments from ODP Site 1146 (Fig. 2, Table 2). The >6 μm silt and SiO_2-enriched sediment fractions have been used to indicate the influence of eolian dust to the northern South China Sea (Wang et al., 1999b; Wehausen and Brumsack, 2002), although it is clear that not all >6 μm terrigenous materials are eolian origin. Moreover, quartz and feldspar (average ~80%) are the two dominant minerals in the loess deposits of Central China (Liu, 1966) and have been transported to the northern South China Sea by the strong East Asian winter monsoon from the Asian inland (Wang et al., 2000) (Fig. 7). A study of mineral aerosols from the low atmosphere of the Eastern China Seas shows that quartz plus feldspar account for 60–80% of the total flux (Li, 1997). If we assume a value of 20% for the average eolian contribution to terrigenous sediments at ODP Site 1146, and 60–80% (quartz+feldspar) content for eolian dust (Li, 1997) and 30% (quartz+feldspar) content for

Table 2
Contribution of eolian dust and fluvial minerals to the terrigenous mineral composition at ODP Site 1146

Source	Total contribution	Relative (Q+F)	Absolute (Q+F)	(Q+F) contribution	Relative clay	Absolute clay	Clay contribution
	(%)—EMM	(%)	(%)	(%)	(%)	(%)	(%)
Eolian dust	**20**	**60–80**	12–16	40–53	**40–20**	8–4	11–6
Fluvial mineral	**80**	23–18	18–14	60–47	72–73	62–66	89–94
Site 1146	**100**		**30**	**100**		**70**	**100**

Note: Bold denotes original data and others are calculated values. Data of mineral composition of eolian dust after Li (1997).

ODP Site 1146 terrigenous sediment. We then calculate that 40–53% of the total (quartz+feldspar) but only 6–11% of the total clay may be originated from eolian supply at ODP Site 1146 (Table 2).

4.2. Implication of the proxies

The paleoclimatic interpretation of mineralogical and sedimentological records requires knowledge of the potential source areas as well as mode and strength of the transport processes involved (e.g., Gingele et al., 1998; Liu et al., 2003). In addition, identification and elimination of the influence of non-monsoon factors, such as tectonic activity on the proxies is another key to interpreting the reconstructed evolution of the East Asian monsoon on a long-term timescale. Here we explain the implication of some monsoon proxies, and then discuss the possible influence of non-monsoon factors on the selected proxies.

Among many mineralogical and sedimentologic proxies, eolian MAR is relatively robust because it is not influenced by local tectonic activity or sea-level change, and indicates the aridity of continental Asia—the source region of eolian dust. Through end-member modeling, variation in MAR of the coarsest end-member EM1 can be used to reconstruct the changing East Asian winter monsoon intensity. The variation in the proportion of EM1 in the terrigenous materials can be used to reconstruct the change of intensity of eolian supply relative to fluvial input, and thus potentially the change of intensity of the winter monsoon relative to the summer monsoon.

Multiple sources and transport processes for the terrigenous sediments at ODP Site 1146 suggest the clay mineral assemblages at ODP Site 1146 were not only controlled by the continental weathering regimes surrounding the South China Sea, but also by the changing strength of the transport processes (Liu et al., 2003; Boulay et al., 2005). The clay mineral record since 2 Ma has been used to trace summer and winter monsoon variability, which in turns is linked to the intensity of the surface ocean currents in the South China Sea (Liu et al., 2003). The prevailing southwesterly surface currents driven by enhanced summer monsoon winds must transport increased smectite from Luzon, whereas prevailing southward nearshore currents driven by enhanced winter monsoon winds would transport more illite and chlorite from the Pearl River and Taiwan to ODP Site 1146 (Liu et al., 2003) (Fig. 7).

Illite and chlorite are considered primary minerals, whose presence in the sediment reflects decreasing hydrolytic processes in continental weathering and an increase of direct rock erosion under cold and arid climatic conditions. In contrast, smectite is readily derived from the chemical weathering of volcanic rocks (e.g., Chamley, 1989; Liu et al., 2004). A strengthened winter monsoon would be expected to produce more illite and chlorite in South China and Taiwan, but little smectite in Luzon. Thus, we can apply the ratio of (illite+chlorite)/smectite as a proxy to reconstruct the evolution of East Asian winter monsoon intensity relative to summer monsoon intensity since the middle Miocene. Relatively high (illite+chlorite)/smectite ratios reflect strongly intensified winter monsoon relative to summer monsoon, in contrast, lower ratios indicate a strengthened summer monsoon relative to winter monsoon.

The weight percent of (quartz+feldspar) in the terrigenous materials can be used as another proxy to trace the history of the East Asian monsoon. As discussed above, 40–53% quartz and feldspar minerals of the terrigenous materials at ODP Site 1146 were transported by winter monsoon circulation from the Chinese Loess Plateau or other exposed arid land in Asia. Hence a strengthened winter monsoon should transport more eolian quartz and feldspar to ODP Site 1146 (Fig. 7). In addition, according to studies of similar sediments (e.g., Wang et al., 1999b; Wehausen and Brumsack, 2002), clay minerals are preferably transported by rivers into the South China Sea. Thus the clay minerals could represent the intensity of the sediment discharge of the continental rivers surrounding the South China Sea and, in turn, the East Asian summer monsoon intensity. An increased

weight percent of quartz and feldspar relative to clay minerals should indicate an intensified winter monsoon relative to summer monsoon.

In contrast, an increased weight percent of clay minerals relative to quartz and feldspar would imply a strengthened summer relative to winter monsoon intensity. Higher contents of quartz, feldspar, SiO_2/Al_2O_3 and SiO_2/K_2O ratios during glacial stages with stronger winter monsoon than during interglacial periods have been documented in the sediments from the northern and southern South China Sea (Boulay et al., 2003; Tamburini et al., 2003; Liu et al., 2004). Consequently, the weight percent of (quartz+feldspar) in terrigenous minerals should be a good proxy for tracing the variational intensity of winter monsoon relative to summer monsoon.

In addition, we argue that the mean grain size of terrigenous materials can be considered as a proxy for paleo-monsoon evolution. On one hand, the mean grain size of terrigenous materials at ODP Site 1146 is effectively controlled by the relative proportion of the coarsest grain-size fraction, and to some extent, we argue that the coarser grain-size fraction corresponds to eolian dust. A stronger winter monsoon would be expected to bring more coarse dust to the study site. As a result mean grain size of terrigenous particles can be used to trace the evolving intensity of winter relative to summer monsoon. However, since 20 Ma, mean grain-size changes are closely correlated to the weight percent of (quartz+feldspar) in terrigenous minerals (Fig. 11), suggesting that the coarser fraction is mainly controlled by quartz and feldspar input and the mean grain size of terrigenous

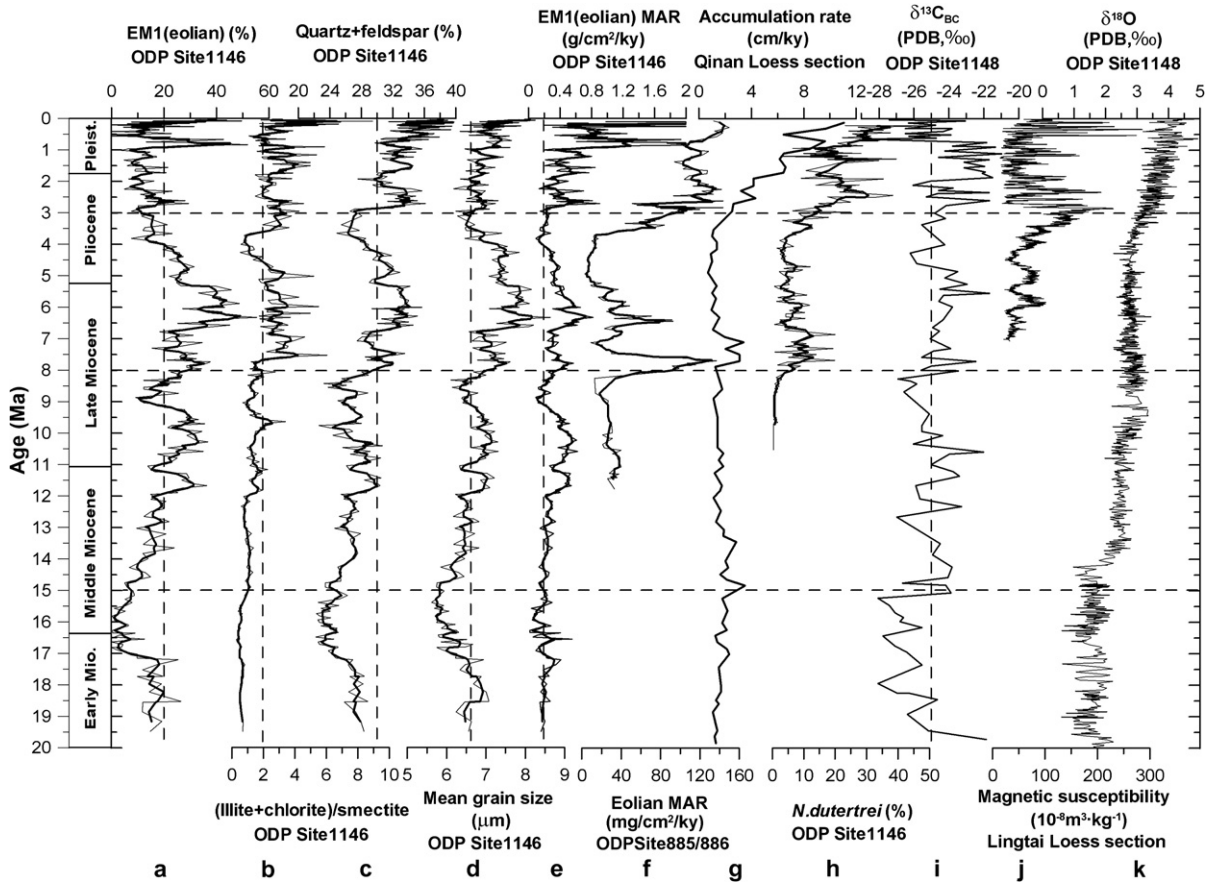

Fig. 11. Marine and terrestrial records since 20 Ma from the South China Sea, the north Pacific and Chinese Loess Plateau. Three dashed lines mark the three profound shifts of the East Asian monsoon intensity at 15 Ma, 8 Ma and 3 Ma. The time series are: (a–e) the coarsest end-member EM1%, (illite+chlorite)/smectite, (quartz+feldspar)%, mean grain size, and EM1 MAR at ODP Site 1146 from this study; (f) eolian MAR from north Pacific ODP Sites 885/886 (Rea et al., 1998); (g) dust accumulation rates of QA-I at Qinan on the Loess Plateau (Guo et al., 2002); (h) Neogloboquadrina dutertrei % at ODP Site 1146 (Wang et al., 2003; Zheng et al., 2004); (i) isotopic composition of black carbon at ODP Site 1148 (Jia et al., 2003); (j) magnetic susceptibility from the Lingtai section on the Loess Plateau (Ding et al., 2001); (k) benthic $\delta^{18}O$ at ODP Site 1148 (Cheng et al., 2004). The data (fine) were smoothed by a three-point moving average (coarse).

materials can be used as another monsoon intensity proxy.

At the same time, the possible effects of tectonic activity, sea-level change, and even global change on paleo-monsoon proxies should also be considered. As discussed above, the end of seafloor spreading in the South China Sea is a period of strong tectonic activity around the South China Sea, which intensified continental erosion and drove enhanced delivery of sediment by rivers to the northern South China Sea (Fig. 7). Therefore, except for the MAR of the coarsest end-member EM1 (eolian), EM1 proportion within the terrigenous sediment fraction, (illite+chlorite)/smectite, (quartz+feldspar)% and mean grain size cannot be used to indicate the evolution of the East Asian monsoon between 17.5 and 15 Ma.

Uplift and erosion of Taiwan is caused by the collision of the Luzon arc with the Eurasian margin. The initial Taiwan arc-continent collision is manifested by multiple stratigraphic records with a wide spectrum of "collision" ages from 16 to 2 Ma (Huang et al., 2006). Assuming that Taiwan or the Yangtze River are sediment sources for ODP Site 1146, the formation of proto-Taiwan since 16–15 Ma should block at least part of the southward supply of suspended particles from the East China Sea and increase the Taiwan related sediments to the study area at the same time.

In any case, the lack of any sedimentation pulse at ODP Site 1146 between 15–3 Ma and 20–17.5 Ma (Fig. 3), the similar clay composition (Table 1 and Fig. 8) and transport process of suspended sediments from Taiwan or the East China Sea by winter monsoon induced southward currents (Fig. 7) suggest that our selected proxies can still be used to indicate the evolution of the East Asian monsoon between 15–3 Ma and 20–17.5 Ma. In addition, two recent uplift episodes of Dongsha islands have been proposed to correlate with two main collision phases between Taiwan and the continental margin of East China at 5–3 and 3–0 Ma and have contributed to the increase in the supply of terrestrial material at 3 and 0.25 Ma (Lüdmann et al., 2001). However, it seems unlikely that the increased sedimentation rate at about 3 Ma just reflects a local event because a similar increase can be found not only in records from ODP Sites 1143, 1146, and 1148 (Wan, 2006), but also in many continental margins, such as the Mississippi delta and its surroundings, the North Sea, several basins offshore southeast Asia, Nova Scotia, and the Vøring plateau off Norway, possibly resulting from global climate instability (Zhang et al., 2001).

The tectonic evolution of Luzon is very complex and here we accepted the Hall (2002) interpretation of a northward extension of the Luzon Arc since the early Miocene resulted from the continuous subduction of the Philippine Sea plate beneath the Eurasian plate. The evolution of the Philippines Archipelago (including Luzon Arc) is shown in Fig. 7. As discussed above, the Luzon Arc may have contributed about 14% of the lithic fraction to ODP site 1146 since 20 Ma if we assume most of smectite at Site 1146 was derived from Luzon. However, it is noteworthy that the smectite MAR at ODP Site 1146 was very stable between 20 and 3 Ma except a very high MARs interval of 17.5–15 Ma (Fig. 4), implying the northward movement of Luzon has no significant influence on the influx of smectite to the study area. Surface sediments east of the coast of Luzon are very rich in smectite, because of large volume of volcanic rocks (e.g., Chen, 1978). The most important passage connecting the South China Sea and the Pacific is the Luzon Strait. It has been long known that there is a year-round intrusion of Kuroshio Current, a bifurcation of the North Equatorial Current, from the Western Pacific into the South China Sea through the Luzon Strait (e.g., Xue et al., 2004) (Fig. 1). The large-scale circulation patterns of the North Equatorial Current and Kuroshio has not changed significantly in the Neogene (Kennett et al., 1985). As a result the intrusion of the Kuroshio Current into the South China Sea through the Luzon Strait could have prompted the transport of smectite-enriched sediments from Luzon into the South China Sea. Subsequently transportation of clay minerals is largely controlled by the monsoon-driven surface circulation in the South China Sea. Therefore, variation of clay minerals at ODP Site 1146 since 20 Ma can be used to trace the evolution of the East Asian monsoon.

Shelf transgression and regression occurring during periods of sea-level change on orbital time scale could have an important influence on sedimentation on the northern margin of the South China Sea (Boulay et al., 2003). Regional sea level in the South China Sea gradually fell from 15 Ma to 10 Ma and then gradually ascended until about 5 Ma (Fig. 3; Haq et al., 1987; Li et al., 2005). As a result, sedimentation rates on the deep water continental margins would be expected to peak around 10 Ma, assuming that the sediment yield in the drainage basin remained constant. However, between 15 and 3 Ma there is no remarkable change in any of the MARs in total terrigenous materials, quartz, feldspar and clay minerals at ODP Sites 1146 (Fig. 3) and 1148 (Clift, 2006). Sediment budgets for the major basin systems in the Asian marginal seas also show that the total flux of clastic material from Asia into the surrounding marginal seas is mostly controlled by the

erosional response to monsoonal precipitation and uplift of Tibet, not to global eustacy (Clift et al., 2004). Thus, there is no significant influence of sea-level change amplitudes on the sedimentation rate at ODP Site 1146 over a million year time scale. In contrast, the frequency and rate of sea-level and climate change are probably of higher importance. During the last 3 Ma, the sea-level change frequency is greatly higher than that before 3 Ma (Fig. 3) and thus the rate of horizontal reworking along the newly exposed shelf increased. Moreover, Zhang et al. (2001) suggested that disequilibrium states of frequent and abrupt changes in temperature, precipitation and vegetation should be effective in causing continental erosion, but only after 4–3 Ma, as global climate deteriorated. Therefore, the increased sedimentation rate in the South China Sea since 3 Ma reflects global climate deterioration as expressed in strong and rapid monsoon variation (Wan et al., 2006).

The variation of MAR of the coarsest end-member EM1 (eolian dust) at ODP Site 1146 clearly shows the enhancement of the East Asian winter monsoon intensity and continental aridity on the Asian inland between 15–10 Ma, 8–4 Ma and since 3 Ma. A similar record of eolian dust deposition was reconstructed at ODP Site 885/886 in the north Pacific (Rea et al., 1998). Studies in Nd isotopic composition have shown that the eolian dust at ODP Site 885/886 was derived from central Asia by westerly wind (Pettke et al., 2000) and thus recorded the history of Asian drying since 11 Ma (Rea et al., 1998). Because of the great difference in distance of the two ODP sites from central Asia, the values of eolian MARs at ODP Site 1146 are about 10 times higher than those at Site 885/886. However, noticeable is the very similar trend in both records, as well as in loess accumulation rate in Qinan on the Loess Plateau (Guo et al., 2002) (Fig. 11). All these suggest that the three sites have actually recorded the same signal of Asian continental desiccation and further confirm the reliability of our modeled results with the end-member algorithm. In addition, the relatively high proportion of end-member EM1 (eolian) in the terrigenous materials between 12–9 Ma and 8–4 Ma implies a stronger eolian supply relative to fluvial input to the study site at that time and thus strengthened winter monsoon relative to summer monsoon. In contrast, except for the time interval of 0.9–0.7 Ma and 0.15–0 Ma, there is basically no change in EM1% since about 3 Ma (Fig. 11). Because the increased fluvial flux (continental erosion) since 3 Ma reflects enhanced erosion due to global climate deterioration, we can deduce a stronger eolian supply relative to fluvial input induced by summer monsoon since about 3 Ma. In other words, the intensity of winter monsoon was strengthened relative to summer monsoon since 3 Ma.

Moreover, it is noteworthy that the variation of (illite+chlorite)/smectite ratio, (quartz+feldspar)%, and mean grain size of the terrigenous materials since 20 Ma is strikingly similar to that of the EM1 (eolian) MAR, consistent with our model that they are all indicators of climate change except during the period of tectonic activity around the South China Sea between 17.5 and 15 Ma (Fig. 11).

4.3. Evolution of the East Asian monsoon

Based on the above discussion, it appears fairly certain that three profound shifts of the winter monsoon intensity and intensity of the winter monsoon relative to summer monsoon occurred, at ~15 Ma, ~8 Ma and the youngest at about 3 Ma. In contrast, there is a little difficulty in understanding the evolution of the summer monsoon. The increased intensity of the winter relative to summer monsoon does not necessarily mean a weakened summer monsoon, because the summer monsoon can be strengthened along with the winter monsoon. Simultaneous increase in sedimentation rates at ODP Sites 1143, 1146 and 1148 (Wan et al., 2006), as well as in MAR of clay minerals (Fig. 3) and the finer end-members EM2+EM3 (fluvial) (Fig. 9) at ODP Site 1146 since 3 Ma, may be the erosional response to both global climatic deterioration and the strengthening of the East Asian summer monsoon after about 3 Ma. It is possible that the summer monsoon intensified simultaneously with the winter monsoon at 3 Ma (e.g., An et al., 2001; Wan et al., 2006).

An enhancement of the South Asian monsoon (Indian monsoon) at about 8 Ma has been proposed based on evidence for increased upwelling in the Arabian Sea (Kroon et al., 1991; Prell et al., 1992) and the eastern Indian Ocean (Singh and Gupta, 2004), as well as a shift from C_3- to C_4-type vegetation in the Indian foreland (Quade et al., 1989). By comparison, reconstruction of the East Asian monsoon mainly comes from studies of loess deposits and recent research following ODP Leg 184 in the South China Sea. Basal dates from the prevailing eolian Red Clay sediments in the Chinese Loess Plateau indicate onset of rapid eolian dust accumulation at about 8 Ma (An et al., 2001; Ding et al., 2001; Lu et al., 2001; Qiang et al., 2001). The onset of Asian desertification has been dated to 22 Ma (Guo et al., 2002) and the broad scale climatic and botanical zones of China appear to be relatively stable since the Oligocene–Miocene boundary (Sun and Wang, 2005), implying a much earlier monsoon than previously thought.

Nonetheless, eolian sedimentation in the Loess Plateau (Guo et al., 2002) and North Pacific (Rea et al., 1998) increased sharply at about 15 Ma, 8 Ma and 3 Ma (Fig. 11) as well as in West and North China (Fang et al., 1997; Ma et al., 1998; Wang et al., 1999a; Sun et al., 2005). These data imply that Asian aridification intensified at about 15 Ma, 8 Ma and 3 Ma, possibly accompanied by a strongly intensified East Asian winter monsoon. The predominant stronger winter monsoon relative to summer monsoon at 8 Ma, as reflected by our proxy records presented here (Fig. 11), is consistent with the general initiation of Asian aridification and eolian dust accumulation in the Chinese Loess Plateau at that time.

In the South China Sea, the percentage of planktonic foraminifer *Neogloboquadrina dutertrei* has been used as a proxy for monsoon-related high productivity. The abrupt increase of *N. dutertrei* % at ODP Site 1146 at about 8 Ma and further rapid increase since 3 Ma suggest enhancement of the East Asian monsoon at 8 Ma and 3 Ma (Fig. 11, Wang et al., 2003; Zheng et al., 2004). $\delta^{13}C$ of black carbon is a proxy for plant metabolism (C3 versus C4 plants) associated with monsoon climate and the relatively heavy $\delta^{13}C$ values of black carbon at 15 Ma, 8 Ma and 3 Ma at ODP Site 1148 in the South China Sea imply the intensification of monsoon climate (Fig. 11, Jia et al., 2003). In addition, a strengthening of the East Asian monsoon at about 8 Ma has been inferred from records of radiolarians (Chen et al., 2003), alkenone stratigraphy (Mercer and Zhao, 2004), minerals and biogenic opal (Wan et al., 2006) from sediments in the South China Sea. Recent evidence supports an enhancement of East Asian monsoon intensity and aridity at about 3 Ma both from onshore (e.g., Sun et al., 1998; An et al., 2001; Ding et al., 2001; Qiang et al., 2001; Guo et al., 2002) and marine data (Wehausen and Brumsack, 2002; Tian et al., 2004; Zheng et al., 2004; Hess and Kuhnt, 2005; Wan et al., 2006). Our study is consistent with these other studies.

4.4. Tibetan uplift and climate change

Numerical climate modeling suggests that the uplift of the Tibetan Plateau may have played a significant role in strengthening the Asian monsoon and Asian aridification through modulating the atmospheric circulation and its barrier effect to southern moisture (e.g., Ruddiman and Kutzbach, 1989; An et al., 2001). Although various proxy records have been interpreted as indicating that the monsoons started or strongly intensified at 10–8 Ma (e.g., Quade et al., 1989; An et al., 2001), a series of studies (Ramstein et al., 1997; Guo et al., 2002; Jia et al., 2003; Sun and Wang, 2005; Clift, 2006) now suggest that the Asian monsoon initiated much earlier than previously thought, possibly since the Oligocene–Miocene boundary. Although the Tibetan uplift history is far from clear at present (e.g.,

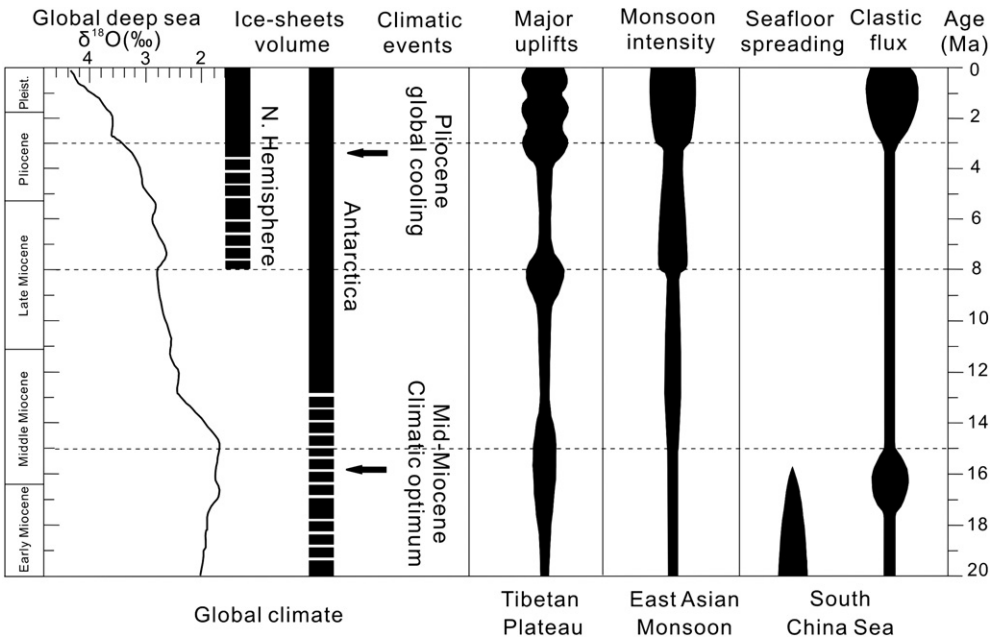

Fig. 12. Schematic model showing variation of global climate (Zachos et al., 2001), major uplifts of the Tibetan Plateau (Li, 1991; Copeland, 1997; Zheng et al., 2000; Tapponnier et al., 2001), the East Asian monsoon intensity and the South China Sea evolution (Lee and Lawver, 1994; Li et al., 2005).

Molnar, 2005; Harris, 2006), it appears credible for the model of a plateau growing northward progressively through time following the Eocene India–Asia collision (e.g., Tapponnier et al., 2001). If that is the case, different stages of growth of the plateau could have contributed to trigger or enhance different climatic effects at different times after the plateau had attained a critical minimum elevation and/or size (e.g., Ramstein et al., 1997, An et al., 2001; Fig. 12).

The gradual enhancement of the East Asian winter monsoon relative to summer monsoon and aridity of the Asian continent at ~15 Ma possibly relates to the global cooling and the onset of Antarctic glaciation (Zachos et al., 2001), as well as the uplift of the southern and perhaps central Tibetan Plateau at that time (e.g., Copeland, 1997; Harris, 2006; Fig. 12). The period around 8 Ma has been suggested as the end of a phase of buildup of the East Antarctic ice sheet and possibly the beginning of the formation of the West Antarctic and Arctic ice sheets (Zachos et al., 2001; Fig. 12). Gupta et al. (2004) argued that global cooling and the increase in volume of the Antarctic ice sheets at 10–8 Ma strengthened wind regimes throughout the Indian Ocean. However, the stable isotope $\delta^{18}O$ at ODP Site 1148 (Fig. 11), as well as the global compilation of deep-sea oxygen isotope records (Zachos et al., 2001) (Fig. 12) remains stable or slight heavier through 8 Ma. At the same time all winter monsoon proxies increase abruptly. These proxies decrease after 5 Ma and reach their minimum at about 4 Ma (Fig. 11), although the global $\delta^{18}O$ values remain slight heavier. Therefore, the enhancement of the East Asian monsoon at 8 Ma cannot be explained by global cooling.

It is recognized that the strength of the monsoon is coupled to the intensity of Northern Hemisphere glaciation (e.g., Wang et al., 2000, 2005), as also reflected in the monsoon proxies and $\delta^{18}O$ record at ODP Site 1148 (Fig. 11), making it unclear whether it is Tibetan altitude, or global climate change, or a combination of both processes that is triggering the strong monsoon at 3–4 Ma. It is possible that additional uplift of Tibet at 3–4 Ma may have strengthened the monsoon and driven glaciation, and in turn the enhanced glaciation may have influenced the development of the Asian monsoon.

5. Conclusions

Detailed analysis of the content and mass accumulation rate of terrigenous minerals in association with clay mineralogy and grain size of terrigenous materials were carried out on 275 samples from ODP Site 1146 in the northern South China Sea in order to obtain proxy records of the East Asian monsoon evolution since 20 Ma.

End-member modeling of a data set of grain-size distributions ($n=273$) results in three end members. The coarsest end-member EM1 is interpreted as eolian dust, the middle and finest end member as fluvial fine silt and fluvial mud, respectively. We estimate that eolian dust (EM1) from the arid Asian inland and fluvial input have contributed on average 20% and 80% of total material to ODP Site 1146, respectively. The terrigenous component in ODP Site 1146 sediments comprises quartz, feldspar and four principal clay minerals (smectite, illite, chlorite and kaolinite). Moreover, about 40–53% of the total (quartz+feldspar), but only 6–11% of the total clay may be derived by eolian supply. Clay minerals are in the majority and are mainly transported by monsoon-induced surface currents from the land masses surrounding the northern South China Sea. Specifically, smectite at ODP Site 1146 mostly comes from the Luzon, kaolinite from the Pearl River, and illite and chlorite mainly from the Pearl River, Taiwan and/or the Yangtze River.

The coarsest end-member EM1 (eolian) proportion and MAR, ratios of (illite+chlorite)/smectite, (quartz+feldspar)% and mean grain-size of terrigenous materials at ODP Site 1146 were adopted as proxies for East Asian monsoon evolution. The consistent variation of these proxies since 20 Ma shows that three profound shifts of the East Asian winter monsoon intensity, degree of Asian continental aridity, and the intensity of winter monsoon relative to summer monsoon occurred, at 15 Ma, 8 Ma and 3 Ma. In comparison, summer monsoon possibly simultaneously intensified with the winter monsoon at 3 Ma. The phased uplift of the Himalaya–Tibetan plateau may have played a significant role in strengthening the Asian monsoon at 8 Ma and possibly 15 Ma and 3 Ma. However, as the strength of the East Asian monsoon is coupled to the intensity of Northern Hemisphere glaciation after about 3 Ma, it remains unclear whether it is the Tibetan altitude or global climate change that is triggering the strong monsoon we see at 3 Ma.

Acknowledgments

This research used samples at ODP Site 1146 provided by the Ocean Drilling Program (ODP). ODP is sponsored by the U.S. National Science Foundation (NSF) and participating countries under management of Joint Oceanographic Institutions (JOI), Inc. We especially thank two anonymous reviewers for thorough and helpful reviews. We thank Dr. K.H. Xu and X.L. Luo for kindly providing the samples from Taiwan and the Pearl River, respectively. Dr. G.J. Weltje is thanked for providing the end-member modeling algorithm. Funding for this research was supported by the National Fundamental

Research and Development Planning Project (Grant No. 2007CB411703), National Natural Science Foundation of China (Grant No. 40576032) and major program of Knowledge Innovation Project of The Chinese Academy of Sciences (Grant No. KZCX2-YW-211).

References

An, Z.S., Kutzbach, J.E., Prell, W.L., Porter, S.C., 2001. Evolution of Asian monsoons and phased uplift of the Himalaya–Tibetan Plateau since late Miocene times. Nature 411, 62–66.

Biscaye, P.E., 1965. Mineralogy and sedimentation of recent deep-sea clay in the Atlantic Ocean and adjacent seas and oceans. Geological Society of America Bulletin 76, 803–832.

Boulay, S., Colin, C., Trentesaux, A., Pluquet, F., Bertaux, J., Blamart, D., Buehring, C., Wang, P., 2003. Mineralogy and sedimentology of Pleistocene sediment in the South China Sea (ODP Site 1144). In: Prell, W.L., Wang, P., Blum, P., Rea, D.K., Clemens, S.C. (Eds.), Proceedings of the Ocean Drilling Program, Scientific Results, vol. 184, pp. 1–21. [Online]. Available from World Wide Web: http://www-odp.tamu.edu/publications/184_SR/VOLUME/CHAPTERS/211.PDF.

Boulay, S., Colin, C., Trentesaux, A., Frank, N., Liu, Z., 2005. Sediment sources and East Asian monsoon intensity over the last 450 ky. Mineralogical and geochemical investigations on South China Sea sediments. Palaeogeography, Palaeoclimatology, Palaeoecology 228, 260–277.

Boulay, S., Colin, C., Trentesaux, A., Clain, S., Liu, Z., Lauer-Leredde, C., 2007. Sedimentary responses to the Pleistocene climatic variation recorded in the South China Sea. Quaternary Research 68, 162–172.

Briais, A., Patrait, P., Tapponnier, P., 1993. Updated interpretation of magnetic anomalies and seafloor spreading stages in the South China Sea: implications for the Tertiary tectonics of SE Asia. Journal of Geophysical Research 98 (B4), 6299–6328.

Chamley, H., 1989. Clay Sedimentology. Springer-Verlag, Berlin.

Chamley, H., Angelier, J., Teng, L.S., 1993. Tectonic and environmental control of the clay mineral sedimentation in the Late Cenozoic orogen of Taiwan. Geodinamica Acta 6, 135–147.

Chen, P.Y., 1978. Minerals in bottom sediments of the South China Sea. Geological Society of American Bulletin 89, 211–222.

Chen, M.H., Wang, R.J., Yang, L.H., Han, J.X., Lu, J., 2003. Development of East Asian summer monsoon environments in the late Miocene: radiolarian evidence from Site 1143 of ODP Leg 184. Marine Geology 201, 169–177.

Cheng, X.R., Zhao, Q.H., Wang, J.L., Jian, Z.M., Xia, P., Huang, B., Fang, D., Xu, J., Zhou, Z., Wang, P., 2004. Data report: stable isotopes from sites 1147 and 1148. In: Prell, W.L., et al. (Eds.), Proceedings of the Ocean Drilling Program, Scientific Results, vol. 184, pp. 1–12. [Online]. Available from World Wide Web: http://www-odp.tamu.edu/publications/184_SR/VOLUME/CHAPTERS/223.PDF.

Clift, P.D., 2006. Controls on the erosion of Cenozoic Asia and the flux of clastic sediment to the ocean. Earth and Planetary Science Letters 241, 571–580.

Clift, P.D., Lee, J.I., Clark, M.K., Blusztajn, J., 2002. Erosional response of South China to arc rifting and monsoonal strengthening; a record from the South China Sea. Marine Geology 184, 207–226.

Clift, P.D., Layne, G.D., Blusztajn, J., 2004. The erosional record of Tibetan uplift in the East Asian marginal seas. In: Clift, P.D., Wang, P., Hayes, D., Kuhnt, W. (Eds.), Continent–Ocean Interactions in the East Asian Marginal Seas. American Geophysical Union, Monograph, vol. 149, pp. 255–282.

Copeland, P., 1997. The when and where of the growth of the Himalaya and the Tibetan Plateau. In: Ruddiman, W.F. (Ed.), Tectonic Uplift and Climate Change. Plenum Press, New York, pp. 19–40.

Dauphin, J.P., 1980. Size distribution of chemically extracted quartz used to characterize fine-grained sediments. Journal of Sedimentary Petrology 50, 205–214.

Davis, J.C., 1973. Statistics and Data Analysis in Geology. John Wiley and Sons Inc., Singapore.

Ding, Z.L., Yang, S.L., Sun, J.M., Liu, T.S., 2001. Iron geochemistry of loess and red clay deposits in the Chinese Loess Plateau and implications for long-term Asian monsoon evolution in the last 7.0 Ma. Earth and Planetary Science Letters 185, 99–109.

Duce, R., Liss, P., Merrill, J., Atlas, E., Buat-Ménard, P., Hicks, B., Miller, J., Prospero, J., Arimoto, R., Church, T., Ellis, W., Galloway, J., Hansen, L., Jickells, T., Knap, A., Reinhardt, K., Schneider, B., Soudine, A., Tokos, J., Tsunogai, S., Wollast, R., Zhou, M., 1991. The atmospherical input of trace species to the world ocean. Global Biogeochemical Cycles 5, 193–259.

Fang, X.M., Xi, X.X., Li, J.J., Mu, D.F., 1997. Discovery of the late Miocene aridity events in West China and its significance. Chinese Science Bulletin 42, 2521–2524 (in Chinese).

Gibbs, R.J., 1977. Clay mineral segregation in the marine environment. Journal of Sedimentary Petrology 47, 237–243.

Gingele, F.X., Müller, P.M., Schneider, R.R., 1998. Orbital forcing of freshwater input in the Zaire Fan area-clay mineral evidence from the last 200 kyr. Palaeogeography, Palaeoclimatology, Palaeoecology 138, 17–26.

Guo, Z.T., Ruddiman, W.F., Hao, Q.Z., Wu, H.B., Qiao, Y.S., Zhu, R.X., Peng, S.Z., Wei, J.J., Yuan, B.Y., Liu, T.S., 2002. Onset of Asian desertification by 22 Myr ago inferred from loess deposits in China. Nature 416, 159–163.

Guong, Z., Jin, Q., Qiu, Z., Wang, S., Meng, J., 1989. Geology, tectonics and evolution of the Pearl River Mouth Basin. In: Zhu, X. (Ed.), Chinese Sedimentary Basins. Elsevier, Amsterdam, pp. 181–196.

Gupta, A.K., Singh, R.K., Joseph, S., Thomas, E., 2004. Indian Ocean high-productivity event (10–8 Ma): linked to global cooling or to the initiation of the Indian monsoons? Geology 32, 753–756.

Hall, R., 2002. Cenozoic geological and plate tectonic evolution of SE Asia and the SW Pacific: computer-based reconstructions, models and animations. Journal of Asian Earth Sciences 20, 353–431.

Harris, N., 2006. The elevation history of the Tibetan Plateau and its implications for the Asian monsoon. Palaeogeography, Palaeoclimatology, Palaeoecology 241, 4–15.

Haq, B.U., Hardenbol, J., Vail, P.R., 1987. Chronology of fluctuating sea levels since the Triassic. Science 235, 1156–1167.

Hess, S., Kuhnt, W., 2005. Neogene and Quaternary paleoceanographic changes in the southern South China Sea (Site 1143): the benthic foraminiferal record. Marine Micropaleontology 54, 63–87.

Huang, C., Yuan, P.B., Tsao, S., 2006. Temporal and spatial records of active arc-continent collision in Taiwan: a synthesis. GSA Bulletin 118, 274–288.

Jia, G., Peng, P., Zhao, Q., Jian, Z., 2003. Changes in terrestrial ecosystem since 30 Ma in East Asia: stable isotope evidence from black carbon in the South China Sea. Geology 31, 1093–1096.

Jian, Z., Zhao, Q., Cheng, X., Wang, J., Wang, P., Su, X., 2003. Pliocene–Pleistocene stable isotope and paleoceanographic changes in the northern South China Sea. Palaeogeography, Palaeoclimatology, Palaeoecology 193, 425–442.

Kennett, J.P., Keller, G., Srinivasan, M.S., 1985. Miocene planktonic foraminiferal biogeography and paleogeographic development of

the Indo-Pacific region. In Miocene ocean: paleogeography and biogeography. Geological Society of America Memoir 163, 197–236.

Kiely, P.V., Jackson, M.L., 1965. Quartz, feldspar, and mica determination for soils by sodium pyrisulfate fusion. Soil Science Society of American Proceedings 29, 159–163.

Kroon, D., Steens, T., Troelstra, S.R., 1991. Onset of monsoonal related upwelling in the western Arabian Sea as revealed by planktonic foraminifers. In: Prell, W.L., Niitsuma, N., et al. (Eds.), Proceedings of the Ocean Drilling Program, Science Results, vol. 117, pp. 257–263.

Lamy, F., Hebbeln, D., Wefer, G., 1999. High-resolution marine record of climatic change in mid-latitude Chile during the last 28,000 years based on terrigenous sediment parameters. Quaternary Research 51, 83–93.

Lee, T.Y., Lawver, L.A., 1994. Cenozoic plate reconstruction of the South China Sea region. Tectonophysics 235, 149–180.

Li, J.J., 1991. The environmental-effects of the uplift of the Qinghai-Xizang Plateau. Quaternary Science Reviews 10 (6), 479–483.

Li, A.C., 1997. A study on fluxes and composition characteristics of mineral aerosols from the low atmosphere of the Eastern China Seas. PhD Thesis. Chinese Academy of Sciences, China, pp. 46–59.

Li, X.H., Wei, G., Shao, L., Liu, Y., Liang, X., Jian, Z., Sun, M., Wang, P., 2003. Geochemical and Nd isotopic variations in sediments of the South China Sea: a response to Cenozoic tectonism in SE Asia. Earth and Planetary Science Letters 211, 207–220.

Li, Q.Y., Jian, Z.M., Su, X., 2005. Late Oligocene rapid transformations in the South China Sea. Marine Micropaleontology 54, 5–25.

Liu, T.S., 1966. The Composition and Structure of Loess. Beijing, Science Press, pp. 46–56.

Liu, Z.F., Trentesaux, A., Clemens, S.C., Colin, C., Wang, P.X., Huang, B.Q., Boulay, S., 2003. Clay mineral assemblages in the northern South China Sea: implications for East Asian monsoon evolution over the past 2 million years. Marine Geology 201, 133–146.

Liu, Z.F., Colin, C., Trentesaux, A., Blamart, D., Bassinot, F., Siani, G., Sicre, M., 2004. Erosional history of the eastern Tibetan Plateau since 190 kyr ago: clay mineralogical and geochemical investigations from the southwestern South China Sea. Marine Geology 209, 1–18.

Lu, L.Q., Fang, X.M., Mason, J.A., Li, J.J., An, Z.S., 2001. The evolution of coupling of Asian winter monsoon and high latitude climate of Northern Hemisphere—grain evidence from 8.1 Ma loess–red clay sequence on the Chinese central Loess Plateau. Science in China (Series D) 44, 185–191.

Lüdmann, T., Wong, H.K., Wang, P.X., 2001. Plio–Quaternary sedimentation processes and neotectonics of the northern continental margin of the South China Sea. Marine Geology 172, 331–358.

Ma, Y., Li, J., Fan, X., 1998. Vegetation and climate evolution from 30.6–5.0 Ma recorded in red beds at Linxia. Chinese Science Bulletin 43, 301–304 (in Chinese).

Mercer, J.L., Zhao, M., 2004. Alkenone stratigraphy of the northern South China Sea for the past 35 M.Y., Sites 1147 and 1148, ODP Leg 184. In: Prell, W.L., Wang, P., et al. (Eds.), Proceedings of the Ocean Drilling Program, Scientific Results, vol. 184, pp. 1–17. [Online]. Available from World Wide Web: http://www-odp.tamu.edu/publications/184_SR/VOLUME/CHAPTERS/208.PDF.

Milliman, J.D., Meade, R.H., 1983. World wide delivery of river sediment to the oceans. Journal of Geology 91, 1–21.

Molnar, P., 2005. Mio–Pliocene growth of the Tibetan Plateau and evolution of East Asian climate. Palaeontologia Electronica 8 (1) (2A:23p, 625KB).

Petschick, R., Kuhn, G., Gingele, F., 1996. Clay mineral distribution in surface sediments of the South Atlantic: sources, transport, and relation to oceanography. Marine Geology 130, 203–229.

Pettke, T., Halliday, A.N., Hall, C.M., Rea, D.K., 2000. Dust production and deposition in Asia and the north Pacific Ocean over the past 12 Myr. Earth and Planetary Science Letters 178, 397–413.

Prell, W.L., Murray, D.W., Clemens, S.C., Anderson, D.M., 1992. Evolution and variability of the Indian Ocean summer monsoon: evidence from the western Arabian Sea drilling program. In: Duncan, R.A., et al. (Eds.), Synthesis of Results from Scientific Drilling in the Indian Ocean, Geophysical Monograph, vol. 70. American Geophysical Union, Washington, DC, pp. 447–469.

Prins, M.A., Weltje, G.J., 1999. End-member modeling of siliciclastic grain-size distributions: the Late Quaternary record of eolian and fluvial sediment supply to the Arabian Sea and its paleoclimatic significance. In: Harbaugh, J., Watney, L., Rankey, G., Slingerland, R., Goldstein, R., Franseen, E. (Eds.), Numerical Experiments in Stratigraphy: Recent Advances in Stratigraphic and Sedimentologic Computer Simulations. SEPM Special Publication, vol. 62. Society for Sedimentary Geology, pp. 91–111.

Prins, M.A., Postma, G., Weltje, G.J., 2000. Controls on terrigenous sediment supply to the Arabian Sea during the late Quaternary: the Makran continental slope. Marine Geology 169, 351–371.

Qiang, X.K., Li, Z.X., Powell, C.McA., Zheng, H.B., 2001. Magnetostratigraphic record of the Late Miocene onset of the East Asian monsoon, and Pliocene uplift of northern Tibet. Earth and Planetary Science Letters 187, 83–93.

Quade, J., Cerling, T.E., Bowman, J.R., 1989. Development of the Asian monsoon revealed by marked ecologic shift in the latest Miocene of northern Pakistan. Nature 342, 163–166.

Ramstein, G., Fluteau, F., Besse, J., Joussaume, S., 1997. Effect of orogeny, plate motion and land–sea distribution on Eurasian climate change over the past 30 million years. Nature 386, 788–795.

Raymo, M.E., Ruddiman, W.F., 1992. Tectonic forcing of late Cenozoic climate. Nature 359, 117–122.

Rea, D.K., 1992. Delivering of Himalayan sediment to the northern Indian Ocean and its relation to global climate, sea level, uplift, and seawater strontium. In: Duncan, R.A., Rea, D.K., Kidd, R.B., von Rad, U., Weissel, J.K. (Eds.), Synthesis of Results from Scientific Drilling in the Indian Ocean. Geophysical Monograph, vol. 70. American Geophysical Union, Washington, DC, pp. 387–402.

Rea, D.K., Janecek, T.R., 1981. Mass-accumulation rates of the non-authigenic inorganic crystalline (eolian) component of deep-sea sediments form the western mid-Pacific mountains, Deep Sea Drilling Project Site 463. Initial Reports of the Deep Sea Drilling Project 62, 653–659.

Rea, D.K., Snoeckx, H., Joseph, L.H., 1998. Late Cenozoic eolian deposition in the North Pacific: Asian drying, Tibetan uplift, and cooling of the northern hemisphere. Paleoceanography 15, 215–224.

Ruddiman, W.F., Kutzbach, J.E., 1989. Forcing of late Cenozoic northern hemisphere climate by plateau uplift in southern Asia and the American West. Journal of Geophysical Research 94, 18409–18427.

Shao, L., Li, X.H., Wei, G.J., Liu, Y., Fang, D.Y., 2001. Provenance of a prominent sediment drift on the northern slope of the South China Sea. Science in China (Series D) 44, 919–925.

Shao, L., Li, X.H., Wang, P.X., Jian, Z.M., Wei, G.J., Pang, X., Liu, Y., 2004. Sedimentary record of the tectonic evolution of the South China Sea since the Oligocene—evidence from deep sea sediments of ODP Site 1148. Advance in Earth Science 19 (4), 539–544 (in Chinese).

Shi, Y., Dai, X., Song, Z., Zhang, W., Wang, L., 2005. Characteristics of clay mineral assemblages and their spatial distribution of Chinese Loess in different climatic zones. Acta Sedimentologica Sinica 23 (4), 691–695 (in Chinese).

Singh, R.K., Gupta, A.K., 2004. Late Oligocene–Miocene paleoceanographic evolution of the southeastern Indian Ocean: evidence from deep-sea benthic foraminifera (ODP Site 757). Marine Micropaleontology 51, 153–170.

Stuut, J.-B.W., Lamy, F., 2004. Climate variability at the southern boundaries of the Namib (southwestern Africa) and Atacama (northern Chile) coastal deserts during the last 120,000 yr. Quaternary Research 62, 301–309.

Stuut, J.-B.W., Prins, M.A., Schneider, R.R., Weltje, G.J., Jansen, J.H.F., Postma, G., 2002. A 300-kyr record of aridity and wind strength in southwestern Africa: inferences from grain-size distributions of sediments on Walvis Ridge, SE Atlantic. Marine Geology 180, 221–233.

Sun, Y., 2001. Separation of quartz minerals from loess samples. Rock and Mineral Analysis 20, 23–26 (in Chinese).

Sun, Y., An, Z., 2000. Sedimentary interpretation of surface textures of quartz grains from the eolian deposits. Acta Sedimentologica Sinica 18 (4), 506–510 (in Chinese).

Sun, X.J., Wang, P.X., 2005. How old is the Asian monsoon system—palaeobotanical records from China. Palaeogeography, Palaeoclimatology, Palaeoecology 222, 181–222.

Sun, D.H., John, S., An, Z.S., Chen, M.Y., Yue, L.P., 1998. Magnetostratigraphy and paleoclimatic interpretation of a continuous 7.2 Ma Late Cenozoic eolian sediments from the Chinese Loess Plateau. Geophysical Research Letters 25, 85–88.

Sun, Y., Lu, H., An, Z., 2006. Grain size of loess, palaeosol and Red Clay deposits on the Chinese Loess Plateau: significance for understanding pedogenic alteration and palaeomonsoon evolution. Palaeogeography, Palaeoclimatology, Palaeoecology 241, 129–238.

Syers, J.K., Chapman, S.L., Jackson, M.L., 1968. Quartz isolation from rocks, sediments and soils for determination of oxygen isotopes composition. Geochimica et Cosmochimica Acta 32, 1022–1025.

Tamburini, F., Adatte, T., Follmi, K., Bernasconi, S.M., Steinmann, P., 2003. Investigating the history of East Asian monsoon and climate during the last glacial–interglacial period (0–140000 years): mineralogy and geochemistry of ODP Sites 1143 and 1144, South China Sea. Marine Geology 201, 147–168.

Tang, Z., Wang, Y., 1992. Clay minerals distribution in the northern South China Sea. Acta Oceanologica Sinica 14 (1), 64–71 (in Chinese).

Tapponnier, P., Xu, Z., Roger, F., Meyer, B., Arnaud, N., Wittlinger, G., Yang, J., 2001. Oblique stepwise rise and growth of the Tibet Plateau. Science 294, 1671–1677.

Taylor, B., Hayes, D.E., 1983. Origin and history of the South China Sea Basin. In: Hayes, D.E. (Ed.), The Tectonic and Geologic Evolution of Southeast Asian Seas and Islands, vol. 2. Am. Geophys. Union, Washington, DC, pp. 23–56.

Thamban, M., Rao, V.P., Schneider, R.R., 2002. Reconstruction of late Quaternary monsoon oscillations based on clay mineral proxies using sediment cores from the western margin of India. Marine Geology 186, 527–539.

Tian, J., Wang, P.X., Chen, X.R., 2004. Development of the East Asian monsoon and Northern Hemisphere glaciation: oxygen isotope records from the South China Sea. Quaternary Science Reviews 23, 2007–2016.

Wan, S.M., 2006. Evolution of the East Asian monsoon: mineralogical and sedimentologic records in the South China Sea since 20 Ma. PhD Thesis. Qingdao, Institute of Oceanology, Chinese Academy of Sciences.

Wan, S.M., Jiang, H.Y., Li, A.C., 2003. Chemical separation of quartz from marine sediments samples. Marine Geology and Quaternary Geology 23 (3), 123–128 (in Chinese with English abstract).

Wan, S.M., Li, A.C., Clift, P.D., Jiang, H.Y., 2006. Development of the East Asian summer monsoon: evidence from the sediment record in the South China Sea since 8.5 Ma. Palaeogeography, Palaeoclimatology, Palaeoecology 241, 139–159.

Wang, J.L., Fang, X.M., Li, J.J., 1999a. Eolian sand deposits in the northeastern Tibetan Plateau since 15 Ma. Chinese Science Bulletin 44, 1326–1331 (in Chinese).

Wang, L., Sarnthein, M., Erlenkeuser, H., Grimalt, J., Grootes, P., Heilig, S., Ivanova, E., Kienast, M., Pelejero, C., Pflaumann, U., 1999b. East Asian monsoon climate during the late Pleistocene: high-resolution sediment records from the South China Sea. Marine Geology 156, 245–284.

Wang, P.X., Prell, W.L., Blum, P., et al., 2000. Proceedings of the Ocean Drilling Program, Initial Reports, vol. 184. Texas A&M University, College Station, TX 77845-9547, USA, pp. 1–77. [CD-ROM]. Available from: Ocean Drilling Program.

Wang, P.X., Jian, Z.M., Zhao, Q.H., Li, Q.Y., Wang, L.J., Liu, Z.F., et al., 2003. Deep-sea records of the evolution of the South China Sea and the East Asian monsoon. Chinese Science Bulletin 48 (21), 2228–2239.

Wang, P.X., Clemens, S., Beaufort, L., Braconnot, P., Ganssen, G., Jian, Z.M., Kershaw, P., Sarnthein, M., 2005. Evolution and variability of the Asian monsoon system: state of the art and outstanding issues. Quaternary Science Reviews 24, 595–629.

Webster, P.J., Magana, V.O., Palmer, T.N., Shukla, J., Tomas, R.A., Yanai, M., Yasunari, T., 1998. Monsoons: processes, predictability, and the prospects for prediction, in the TOGA decade. Journal of Geophysical Research 103, 14451–14510.

Wehausen, R., Brumsack, H.J., 2002. Astronomical forcing of the East Asian monsoon mirrored by the composition of Pliocene South China Sea sediments. Earth and Planetary Science Letters 201, 621–636.

Wehausen, R., Tian, J., Brumsack, H.J., Cheng, X.R., Wang, P.X., 2003. Geochemistry of Pliocence sediments from ODP site 1143 (Southern South China Sea). In: Wang, P., Prell, W.L., et al. (Eds.), Proceedings of the Ocean Drilling Program, Science Results, vol. 184, pp. 1–25. [Online]. Available from: http://www-odp.tamu.edu/publications/184_SR/VOLUME/CHAPTERS/201.PDF.

Weltje, G.J., 1997. End-member modeling of compositional data: numerical–statistical algorithms for solving the explicit mixing problem. Journal of Mathematical Geology 29, 503–549.

Xiao, J.L., Porter, S.C., An, Z.S., et al., 1995. Grain size of quartz as an indicator of winter monsoon strength on the Loess Plateau of Central China during the last 130000 years. Quaternary Research 43, 22–29.

Xue, H., Chai, F., Pettigrew, N., Xu, D., 2004. Kuroshio intrusion and the circulation in the South China Sea. Journal of Geophysical Research 109, C02017. doi:10.1029/2002JC001724.

Zachos, J.C., Pagani, M., Sloan, L., Thomas, E., Billups, K., 2001. Trends, rhythms, and aberrations in global climate 65 Ma to present. Science 292, 686–692.

Zhang, P., Molnar, P., Downs, W.R., 2001. Increased sedimentation rates and grain sizes 2–4 Myr ago due to the influence of climate change on erosion rates. Nature 410, 891–897.

Zheng, H.B., Powell, C.M., An, Z.S., Zhou, J., Dong, G., 2000. Pliocene uplift of the northern Tibetan Plateau. Geology 28, 715–718.

Zheng, H.B., Powell, C.M., Rea, D.K., Wang, J.L., Wang, P.X., 2004. Late Miocene and mid-Pliocene enhancement of the East Asian monsoon as viewed from the land and sea. Global and Planetary Change 41, 147–155.